



Published in final edited form as:

Cell Rep. 2021 December 14; 37(11): 110124. doi:10.1016/j.celrep.2021.110124.

Control of Foxp3 induction and maintenance by sequential histone acetylation and DNA demethylation

Jun Li^{1,4}, Beisi Xu^{2,4}, Minghong He¹, Xinying Zong¹, Trevor Cunningham¹, Cher Sha¹, Yiping Fan², Richard Cross¹, Jacob H. Hanna³, Yongqiang Feng^{1,5,*}

¹Department of Immunology, St. Jude Children's Research Hospital, Memphis, TN 38105, USA

²Center for Applied Bioinformatics, St. Jude Children's Research Hospital, Memphis, TN 38105, USA

³Department of Molecular Genetics, Weizmann Institute of Science, Rehovot 7610001, Israel

⁴These authors contributed equally

⁵Lead contact

SUMMARY

Regulatory T (T_{reg}) cells play crucial roles in suppressing deleterious immune response. Here, we investigate how T_{reg} cells are mechanistically induced *in vitro* (iT_{reg}) and stabilized via transcriptional regulation of T_{reg} lineage-specifying factor Foxp3. We find that acetylation of histone tails at the *Foxp3* promoter is required for inducing Foxp3 transcription. Upon induction, histone acetylation signals via bromodomain-containing proteins, particularly targets of inhibitor JQ1, and sustains Foxp3 transcription via a global or *trans* effect. Subsequently, Tet-mediated DNA demethylation of *Foxp3* cis-regulatory elements, mainly enhancer CNS2, increases chromatin accessibility and protein binding, stabilizing Foxp3 transcription and obviating the need for the histone acetylation signal. These processes transform stochastic iT_{reg} induction into a stable cell fate, with the former sensitive and the latter resistant to genetic and environmental perturbations. Thus, sequential histone acetylation and DNA demethylation in Foxp3 induction and maintenance reflect stepwise mechanical switches governing iT_{reg} cell lineage specification.

Graphical Abstract

This is an open access article under the CC BY-NC-ND license (<http://creativecommons.org/licenses/by-nc-nd/4.0/>).

*Correspondence: Yong.Feng@stjude.org.

AUTHOR CONTRIBUTIONS

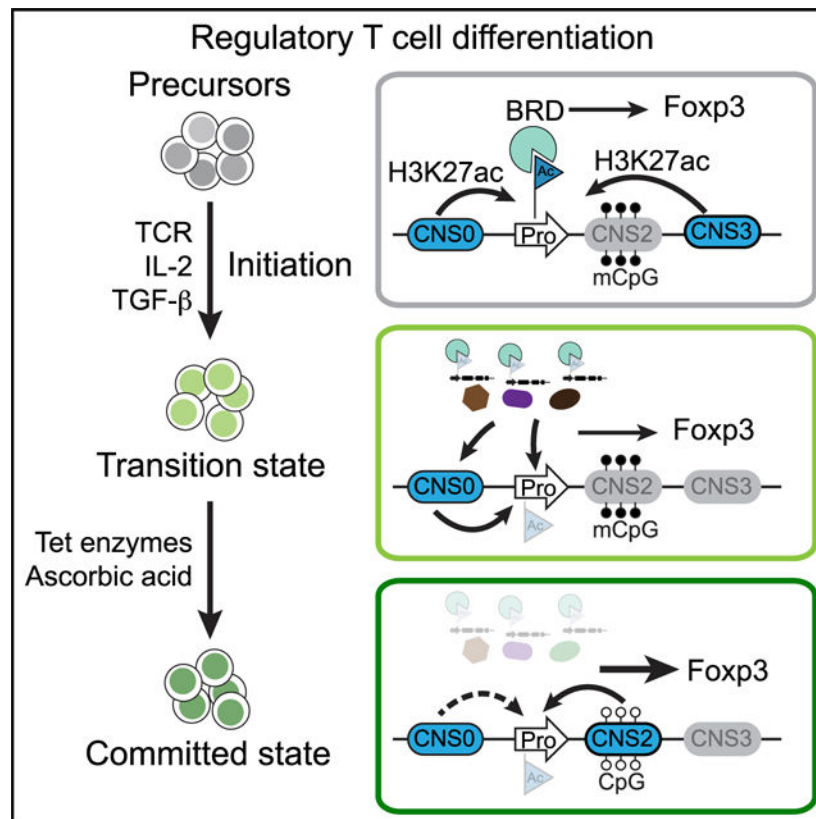
J.L. and Y. Feng. conceived of and designed the experiments and interpreted the results. B.X. and Y. Fan analyzed the high-throughput sequencing data. M.H. performed the Cut&Run experiments and interpreted the results. T.C. and C.S. assisted with iT_{reg} cell induction and stability assays. J.L. and X.Z. quantified nascent Foxp3 mRNA. X.Z. provided critical comments. R.C. assisted with FACS sorting. J.H. provided *Tet1-3^{fl/fl}* mice. J.L. and Y. Feng. wrote the manuscript.

SUPPLEMENTAL INFORMATION

Supplemental information can be found online at <https://doi.org/10.1016/j.celrep.2021.110124>.

DECLARATION OF INTERESTS

The authors declare no competing interests.



In brief

Nuclear protein Foxp3 determines regulatory T cell lineage identity and immunosuppressive function. Li et al. uncover the switches of the transcriptional driving forces of Foxp3 expression during regulatory T cell differentiation *in vitro* governed by sequential histone acetylation and Tet-induced DNA demethylation of *FoXP3* cis-regulatory elements.

INTRODUCTION

T_{reg} cells are induced from precursor cells by T cell antigen receptor (TCR) agonists and favorable environmental cues, including interleukin (IL)-2 and TGF- β , to suppress specific pathogenic T cells and maintain immune homeostasis (Josefowicz et al., 2012; Savage et al., 2020). T_{reg} cells are long-lived and continuously required to maintain immune tolerance (Kim et al., 2007; Rubtsov et al., 2010). Thus, maintenance of a stable lineage in the absence of T_{reg} -induction cues or in adverse environments is critical for sustained T_{reg} suppressive function.

T_{reg} cell lineage commitment and suppressive function rely on nuclear factor Foxp3 (Brunkow et al., 2001; Fontenot et al., 2003; Gavin and Rudensky, 2003; Hori et al., 2003; Liston et al., 2007). A growing list of cell-extrinsic and cell-intrinsic factors was known to regulate Foxp3 induction or stability, among which histone and DNA modifications (hereinafter referred to as epigenetic mechanisms) appear to play important roles (Ohkura and Sakaguchi, 2020). For example, histone acetylation catalyzed by CBP/p300 is

indispensable for T_{reg} cell development and function. Mice with T_{reg}-specific deletion of CBP alone, or together with p300 have significantly less T_{reg} cells (Liu et al., 2014; Liu et al., 2013). Similarly, dynamic regulation of DNA methylation governs both Foxp3 induction and maintenance. In the absence of DNA methyltransferase 1 (Dnmt1), TCR stimulation alone is sufficient to drive Foxp3 induction in precursor cells (Josefowicz et al., 2009). On the other side, active DNA demethylation by Tet methylcytosine dioxygenases is required for the stabilization and maintenance of Foxp3 expression through *Foxp3* enhancer CNS2 (Nakatsukasa et al., 2019; Yue et al., 2019; Yue et al., 2016)(Feng et al., 2014; Li et al., 2014; Zheng et al., 2010).

Given that T_{reg} cell fate determination is a process converting fluctuating induction cues to a committed cell fate, it is important to determine the stage-specific activities of individual epigenetic mechanisms. In the case of histone acetylation widely used to activate gene expression (Marmorstein and Zhou, 2014), it is unclear how this permissive epigenetic mechanism regulates Foxp3 expression through its *cis*-regulatory elements or in *trans* via global gene expression. Histone acetylation may also control T_{reg} cell function independently of Foxp3 expression. Specifying the roles of histone acetylation would produce new mechanistic insights into T_{reg} cell differentiation and function.

Tet-DNA demethylation controls the expression of many genes (Nakatsukasa et al., 2019; Ohkura et al., 2012; Yue et al., 2019), which might stabilize Foxp3 expression in *trans*. It remains to be determined to what extent Tet-dependent *cis* and *trans* mechanisms stabilize Foxp3 transcription. A direct examination of the sufficiency of CNS2 in mediating Tet function would address this basic question. Mechanistically, how DNA demethylation leads to stable Foxp3 transcription in its native genomic context is also unclear.

Here, we examined T_{reg} cell induction, lineage commitment, and maintenance *ex vivo* with mouse primary T cells to determine the stage-specific roles of histone acetylation in controlling Foxp3 expression. We also took advantage of vitamin C or ascorbic acid (ASC)-dependent control of Tet enzymatic activity (Sasidharan Nair et al., 2016; Yue et al., 2016) to probe the mechanisms by which DNA demethylation maintains Foxp3 expression in *cis* through enhancer CNS2.

RESULTS

Histone acetylation is required for Foxp3 induction in *cis*

To understand the epigenetic mechanisms controlling Foxp3 expression during naive CD4 T (T_n) cell differentiation to T_{reg} cells *in vitro* (iT_{reg} cells), which recapitulates T_{reg} cell development *in vivo*, we examined permissive histone acetylation H3K27ac during Foxp3 induction. H3K27ac is deposited by histone acetyltransferases (HATs) and read by bromodomain (BRD)-containing proteins (Fujisawa and Filippakopoulos, 2017). Using Cut&Run sequencing (seq) (Skene and Henikoff, 2017), we confirmed broad H3K27ac around the *Foxp3* promoter in *ex vivo*-isolated natural T_{reg} (nT_{reg}) cells but not in CD4 T_n cells (Figure 1A). We then used pharmacological inhibitors to examine the stage-specific roles of histone acetylation during iT_{reg} cell differentiation. Blockade of HAT CBP/p300 with C646, I-CBP112, or SGC-CBP30 reduced Foxp3 induction efficiency in

a dose-dependent manner (Figures 1B, S1A, and S1B), indicating that histone acetylation signal plays a critical role. To test whether BRD proteins are required to transduce the histone acetylation signal, we treated differentiating T cells with BRD inhibitors JQ1, I-BET151, bromosporine, or PFI-1, resulting in a dose-dependent inhibition of Foxp3 induction (Figures 1C and S1C–S1E).

Conversion of precursor cells to T_{reg} cells is a digital switch manifested by the frequency of Foxp3⁺ cells whereas Foxp3 expression level is a quantitative trait. Next, we tested whether Foxp3 expression level is also controlled by histone acetylation signal during iT_{reg} cell development. We cultured CD4 Tn cells in T_{reg}-induction media containing titrated amounts of JQ1 and analyzed the cells 4 d later. We observed that Foxp3 induction efficiency and expression levels per cell were highly correlated ($R^2 = 0.9975$; Figure 1D), indicating that these two traits of iT_{reg} cells are both controlled by histone acetylation signal via BRD proteins targeted by JQ1.

To confirm the effects of these inhibitors, we performed chromatin immunoprecipitation (ChIP) of H3K27ac followed by quantitative PCR (qPCR) or high-throughput sequencing with neutrally activated CD4 Tn (Th0) cells and CD4 Tn cells cultured in T_{reg}-induction media supplemented with DMSO, C646, or JQ1. We harvested cells 24 h later at the early phase of iT_{reg} cell induction to fully reveal the effects of these inhibitors. C646 treatment resulted in a drastic reduction of H3K27ac level at the *Foxp3* promoter (Figures 1E–1G), consistent with its reported effect on CBP/p300 (Marmorstein and Zhou, 2014). In comparison, JQ1 treatment only caused a relatively milder decrease of H3K27ac level at the *Foxp3* promoter, likely due to an indirect effect. These results further confirmed the overall role of histone acetylation signal in driving Foxp3 induction during iT_{reg} cell development (Feng et al., 2015; Liu et al., 2014).

To test whether histone acetylation signal directly promotes Foxp3 induction, we added JQ1 to culture medium at d 2 during iT_{reg} cell induction and analyzed Foxp3 expression in live cells at d 4. This abruptly reduced Foxp3⁺ cells (Figure 1H), and the remaining Foxp3⁺ cells significantly decreased the expression levels of Foxp3 and its target genes (e.g., CD25, GITR, and CTLA-4; Figure S1F). However, this 2-d JQ1 treatment could still impair Foxp3 induction via a global effect. To solve this issue, we reasoned that the transient transcriptional activity of Foxp3 upon acute JQ1 treatment would reveal the direct role of histone acetylation. To this end, we treated differentiating CD4 Tn cells with JQ1 for 1 h and then pulse chased newly synthesized RNA with ethynyl uridine (EU) (Figure 1I). We quantified EU-labeled Foxp3 nascent mRNA with reverse transcription (RT) followed by quantitative PCR (qPCR). After normalization by the nascent mRNA of *Gapdh*, not affected by JQ1 treatment (not shown), we observed a drastic reduction of Foxp3 nascent mRNA upon acute JQ1 treatment. JQ1 significantly reduced Foxp3⁺ cells regardless of cell proliferation, and acute JQ1 treatment reduced RNA polymerase II (Pol II) binding at the *Foxp3* locus (Figures S1G–S1I). These results suggest that histone acetylation signal via BRD proteins or JQ1 targets promotes Foxp3 transcription in *cis* in a cell cycle-independent manner.

Foxp3 enhancers CNS0, CNS1, and CNS3 have been shown to facilitate Foxp3 induction (Figure 1A) (Dikiy et al., 2021; Feng et al., 2015; Kawakami et al., 2021; Zheng et al., 2010; Zong et al., 2021). CNS3 acts through histone acetylation, at least partially, to enable efficient Foxp3 induction. Because CNS0 and CNS3 coordinate during T_{reg} cell development, we then tested whether histone acetylation also plays a role in CNS0 function. In the absence of CNS0, the *Foxp3* promoter accumulated significantly less H3K27ac at 24 h during iT_{reg} cell development (Figure 1J). At d 4 when iT_{reg} cells were fully induced, CNS0 deficiency did not affect H3K27ac levels at the *Foxp3* promoter, which was comparable to CNS0-sufficient and CNS0-deficient nT_{reg} cells. This result is consistent with the apparent roles of CNS0 and CNS3 in Foxp3 induction but not maintenance (Dikiy et al., 2021). Foxp3 induction was significantly more impaired by C646 or JQ1 treatment in CNS0-deficient versus CNS0-sufficient cells despite their comparable effects on cell viability (Figures 1K, 1L, S1J, and S1K). Thus, histone acetylation of the *Foxp3* promoter is induced by T_{reg}-induction cues likely via the synergistic activity of CNS0 and CNS3 to facilitate Foxp3 induction.

Taken together, these data uncover a critical role of histone acetylation in promoting Foxp3 induction in *cis* during early iT_{reg} cell differentiation.

Histone acetylation signal via BRD proteins targeted by JQ1 is dispensable for stable Foxp3 expression in ASC-treated iT_{reg} cells

Tet-dependent DNA demethylation was proposed as the main mechanism acting in *cis* to “lock in” Foxp3 expression in committed T_{reg} cells. Because this step is not readily accessible for in-depth examination of T_{reg} cell differentiation *in vivo*, we modeled it using differentiating iT_{reg} cells by supplementing the culture medium with ASC that activates Tet enzymes to induce active DNA demethylation (Figure 2A).

We isolated CD4 Tn cells from wild-type (WT) *Foxp3^{3gfp}* knockin mice (Fontenot et al., 2005) and induced iT_{reg} cells in media supplemented with or without ASC. To assess the stability Foxp3 expression, we sorted GFP⁺ iT_{reg} cells 4 d later and cultured them in media containing recombinant IL-2, IL-2 neutralization antibodies (aIL-2), or JQ1 together with immobilized anti-CD3 and anti-CD28 antibodies (Figure 2B). More than 80% of mock-treated iT_{reg} cells lost Foxp3 expression after IL-2 deprivation and approximately 50% of cells maintained Foxp3 expression in the presence of IL-2 (Figure 2C). Remarkably, more than 80% of ASC-treated iT_{reg} cells remained Foxp3⁺ regardless of the culture conditions, resembling stable nT_{reg} cells (Figures 2C, S2A, and S2B). Notably, Foxp3 expression levels were still controlled by IL-2 signaling in ASC-treated iT_{reg} cells. These results suggest that ASC treatment separates the mechanisms controlling the stability and levels of Foxp3 expression.

To further understand Foxp3 transcription during this transition, we pulse chased newly synthesized RNA with EU and compared the transcriptional activity of Foxp3 in mock- and ASC-treated iT_{reg} cells with or without IL-2 deprivation (Figure 2D). IL-2 deprivation slightly reduced Foxp3 transcription in mock-treated iT_{reg} cells, suggesting an accumulative effect of attenuated IL-2 signaling on the stability and levels of Foxp3 expression (Figures

2C and 2E). In contrast, ASC-treatment drastically enhanced the transcriptional activity of Foxp3, suggesting an abrupt change of the mechanisms governing Foxp3 transcription.

Next, we tested whether histone acetylation plays a role in maintaining Foxp3 expression in differentiated iT_{reg} cells. We cultured mock- and ASC-treated iT_{reg} cells in media containing titrated amounts of JQ1. Besides the strong effect on cell viability, JQ1 treatment abruptly silenced Foxp3 expression in live mock-treated iT_{reg} cells (Figure 2F, 2G, S2C, and S2D). In contrast, Foxp3 expression was maintained in more than 70% of ASC-treated live iT_{reg} cells. This effect appears to be independent of cell proliferation. Akin to IL-2 deprivation (Figure 2C), JQ1 reduced Foxp3 expression levels in both mock- and ASC-treated iT_{reg} cells (Figure 2G). Thus, histone acetylation signal via BRD proteins targeted by JQ1 is required to sustain Foxp3 expression prior to ASC-induced epigenetic changes.

To test the requirement for Tet enzymes, we ablated conditional *Tet1*, *Tet2*, and *Tet3* (*Tet1-3^{fl/fl}*) in CD4 Tn cells with retroviral Cre and verified the deletion efficiency with qPCR (Figures 2H and S2E). Neither *Tet1-3* deficiency nor ASC treatment influenced Foxp3 induction (Figure S2F). However, Cre-transduced iT_{reg} cells significantly decreased the stability of Foxp3 expression in ASC-treated iT_{reg} cells after JQ1 treatment or upon IL-2 deprivation (Figure 2I). *Tet* ablation also eliminated ASC-dependent upregulation of Foxp3 and CD25 expression (Figures S2G–S2I). We also measured Foxp3 transcripts with RT-qPCR and observed a profound downregulation of Foxp3 transcription in Cre-transduced iT_{reg} cells regardless of the culture conditions (Figure 2J). These results confirmed the requirement for Tet enzymes in the effect of ASC on iT_{reg} cells.

In summary, our data suggest that Tet-dependent DNA demethylation switches the drivers of Foxp3 transcription, conferring stable iT_{reg} cell identity in adverse environments.

Histone acetylation signal via BRD proteins targeted by JQ1 maintains Foxp3 expression in mock-treated iT_{reg} cells in *trans*

Histone acetylation signal may maintain Foxp3 transcription in *cis* via its promoter or in *trans* via other regulators in mock-treated iT_{reg} cells. To distinguish these two models, we first examined H3K27ac levels at the *Foxp3* promoter in iT_{reg} cells. Although it was significantly lower at the early stage of iT_{reg} cell differentiation in the absence of CNS0, differentiated CNS0-deficient iT_{reg} and mature nT_{reg} cells showed normal H3K27ac levels (Figure 1J). Because mock-treated CNS0-deficient iT_{reg} cells readily lose Foxp3 expression without complete T_{reg}-induction cues (Dikiy et al., 2021), histone acetylation signal appears to be insufficient for maintaining Foxp3 expression in *cis* in these cells.

To test this possibility, we performed SLAM-seq (Muhar et al., 2018) to assess global transcriptional activity upon acute JQ1 treatment (Figure 3A). We induced iT_{reg} cells and 4 d later treated them with JQ1 or DMSO for 5 h, during which 4-thiouridine (4sU) was added for 4 h. Although this protocol did not completely avoid the influence of JQ1 on total RNA transcripts (Figure 3B), we observed a striking effect of acute JQ1 treatment on global transcriptional activities quantified by normalized, 4sU-labeled new mRNAs (Figure 3C). ASC treatment affected the levels of both total and newly synthesized RNAs (Figures 3C and 3D). The former were likely caused by increased or decreased transcriptional activity

(Figures 3D and S3A). Particularly, new Foxp3 transcripts were significantly increased in ASC-treated iT_{reg} cells, consistent with the EU labeling result (Figure 2E) and Foxp3 protein levels per cell (Figures 2G and S2H).

We then examined the effect of JQ1 on new mRNAs (Figures 3E, 3F, S3B, and S3C). Surprisingly, we observed an overall comparable impact ($R^2 \approx 0.8$) of JQ1 in mock- and ASC-treated iT_{reg} cells with or without normalization by total reads (Figures 3E, 3G, and S3D). Foxp3 new transcripts were not significantly changed in JQ1-treated iT_{reg} cells without ASC preexposure (Figure 3E), contrary to unstable, lower Foxp3 expression after long-term JQ1 treatment (Figures 2G, 2I, and 2J). Acute JQ1 treatment also did not affect RNA Pol II, Pol II carboxy terminal domain (CTD) serine 2 phosphorylation, or Pol II CTD serine 5 phosphorylation at the *Foxp3* locus (Figure S3E). As a control, Myc was downregulated by JQ1 in both mock- and ASC-treated iT_{reg} cells, in agreement with a published report (Muhar et al., 2018). These results suggest that histone acetylation signal via BRD proteins targeted by JQ1 is not required for the maintenance of Foxp3 expression in *cis* in differentiated iT_{reg} cells.

To understand how JQ1 destabilized Foxp3 expression in the long term, we examined the genes whose transcriptional activity was affected by JQ1 in iT_{reg} cells. An unbiased analysis showed that several known positive regulators of Foxp3 expression were drastically downregulated in JQ1-treated iT_{reg} cells (e.g., *Bach2*, *Bcl11b*, *Foxp1*, *Il2ra*, *Ptpn22*, *Runx1*, *Runx3*, and *Socs1*; Figure 3H). This result suggests that histone acetylation signal maintains Foxp3 expression in mock-treated iT_{reg} cells by upregulating the expression of these positive regulators. Furthermore, although JQ1 treatment downregulated comparable genes in ASC-treated iT_{reg} cells (Figures 3G and 3H), it did not impair the stability of Foxp3 expression. Thus, this functional transition of histone acetylation in Foxp3 induction and maintenance reflects a key mechanistic switch during iT_{reg} cell differentiation.

To better understand this global effect, we treated iT_{reg} cells with different doses or durations of JQ1 and assessed Foxp3 expression in live cells 3 d later (Figure 3I). We observed a dose- and duration-dependent reduction of the stability and expression levels of Foxp3 in mock-treated iT_{reg} cells (Figures 3J and 3K). This result suggests that histone acetylation signal maintains Foxp3 expression via BRD proteins targeted by JQ1 in mock-treated iT_{reg} cells via an accumulative, global effect.

CNS2 is required for Tet/DNA demethylation-dependent stabilization of Foxp3 expression

To understand how ASC stabilizes Foxp3 expression, we first fine mapped differential DNA methylation sites in CD4 Tn, effector T (Te), nT_{reg}, and mock- and ASC-treated iT_{reg} cells (Figures 4A, S4A, and S4B). Compared to Tn and Te cells, nT_{reg} cells were hypomethylated at *Foxp3* promoter, CNS2, and several other regions in the locus (Figure 4B). ASC induced hypomethylation of these DMRs in iT_{reg} cells to a level comparable to that in nT_{reg} cells. Although many T_{reg}-specific DMRs (e.g., *Lrrc32*, *Il2ra*, and *Ctla4*) were less hypomethylated in ASC-treated iT_{reg} cells (Figure S4C), our results (Figures 4B and S4D–S4F), together with published reports (Sasidharan Nair et al., 2016; Yue et al., 2016), indicate that ASC-treated iT_{reg} cells serve as an excellent *ex vivo* model in which to study DNA demethylation-dependent control of Foxp3 expression.

To verify the requirement for Tet enzymes in ASC-induced hypomethylation of CNS2, we acutely ablated *Tet1-3* with retroviral Cre during iT_{reg} cell development, which abolished the effect of ASC on CNS2 demethylation (Figure 4C), supporting the reported role of ASC and Tet enzymes (Sasidharan Nair et al., 2016; Yue et al., 2016).

To test the sufficiency of CNS2 for ASC-induced stabilization of Foxp3 expression, we examined Foxp3 expression in CNS2-sufficient and CNS2-deficient iT_{reg} cells. In mock-treated iT_{reg} cells, TCR restimulation alone or in combination with JQ1, IL-4, or IL-6 drastically diminished Foxp3⁺ cells in both CNS2-sufficient and CNS2-deficient cells (Figures 4D, 4E, S4G, and S4H). Foxp3 expression in mock-treated CNS2-deficient iT_{reg} cells appeared to be less stable than that in CNS2-sufficient iT_{reg} cells, suggesting a minor role of CNS2 in maintaining Foxp3 expression before DNA demethylation. Alternatively, this effect might be caused by low levels of CNS2 demethylation without supplemented ASC.

ASC treatment drastically stabilized Foxp3 expression in WT iT_{reg} cells regardless of the culture conditions (Figures 4D, 4E, S4G, and S4H). The same treatment only slightly stabilized Foxp3 expression in CNS2-deficient iT_{reg} cells, suggesting that additional genetic elements may also be involved, consistent with a broad hypomethylation of *Foxp3* enhancers in nT_{reg} and ASC-treated iT_{reg} cells (Figure 4B). Quantification of total and nascent Foxp3 transcripts further confirmed that this effect was achieved at the transcriptional level (Figures 4F and 4G). Thus, CNS2 contributes to most, if not all, ASC-dependent stabilization of Foxp3 expression. Our results largely exclude the global or *trans* function of Tet/ASC-induced DNA demethylation in maintaining Foxp3 transcription.

DNA methylation controls chromatin accessibility and nuclear factor binding at CNS2

To understand how CNS2 demethylation controls Foxp3 expression, we first examined H3K27ac levels and observed a significant increase between *Foxp3* promoter and CNS2 upon ASC treatment (Figures 5A and 5B). We then assessed chromatin architecture with ATAC-seq (Buenrostro et al., 2013). Among 3,320 genetic elements with significantly changed accessibility upon ASC treatment, CNS2 became as accessible as that in nT_{reg} cells (Figures 5A and 5C; Samstein et al., 2012), which may facilitate nuclear factor binding. To test this possibility, we assessed Stat5 binding because of its known role in Foxp3 expression. Among 1,127 Stat5-binding sites, 39 were enhanced or attenuated ($p < 0.01$) in ASC-treated iT_{reg} cells (Figures 5A and 5D). Particularly, Stat5 binding at CNS2 was drastically increased upon ASC treatment. In comparison, Stat5 binding at CNS0 was unchanged.

ASC treatment also increased RNA Pol II occupancy at 117 genes ($p < 0.01$) with *Foxp3* on the top (Figures 5A and 5E). Similarly, increased Stat5 and Pol II binding at other genetic elements in iT_{reg} cells upon ASC treatment was associated with reduced DNA methylation and higher levels of H3K27ac (Figures 5F and Figure 5G).

To test whether Stat5 binding at CNS2 was T_{reg} cell specific, we compared mock- and ASC-treated Th0 cells (neutrally activated CD4 Tn cells) and iT_{reg} cells. We observed Stat5 binding at CNS2 in ASC-treated iT_{reg} cells but not in mock-treated iT_{reg} cells or

ASC-treated Th0 cells (Figure 5H). Ablation of *Tet1-3* with retroviral Cre 2 d before ASC treatment eliminated Stat5 binding at CNS2 (Figure 5I), supporting the role of Tet-induced DNA demethylation. We then tested whether this effect also applies to nT_{reg} cells. Because the transition state of DNA demethylation cannot be readily captured *in vivo*, we compared Stat5 binding, chromatin accessibility, and differential DNA methylation. Stat5 binding was highly enriched at hypomethylated, accessible regions in nT_{reg} cells (Figures S5A and S5B), suggesting a causal role of DNA methylation in chromatin accessibility and Stat5 binding.

Increased CNS2 accessibility may also facilitate the binding of other nuclear factors. We then examined Foxp3 association with CNS2, a feedforward loop proposed to stabilize T_{reg} cell fate (Rudensky, 2011). Indeed, Foxp3 binding at CNS2 was drastically increased in ASC-treated *Tet1-3^{fl/fl}* iT_{reg} cells but not in cells transduced with retroviral Cre before ASC treatment (Figure 5J). Notably, CNS2 deficiency did not influence chromatin accessibility around the *Foxp3* locus in iT_{reg} cells or DNA methylation levels in nT_{reg} cells (Figure S5C) (Zong et al., 2021). Taken together, although the factors that differentially bind at CNS2 remain to be fully determined, DNA demethylation appears to rewire the regulatory circuits controlling Foxp3 transcription by modulating the binding of nuclear factors.

Assessment of the role of Foxp3 feedforward loop in maintaining Foxp3 transcription

Next, we attempted to understand these regulatory circuits assembled via hypomethylated CNS2. Stat5 binding at CNS2 appeared to be insufficient to account for stable Foxp3 expression in ASC-treated iT_{reg} cells when IL-2 was deprived (Figure 2C). We then tested whether Foxp3 binding at CNS2 provides a strong feedforward loop in stabilizing Foxp3 transcription. To this end, we used *Foxp3^{loxP}-Thy1.1-Stop-loxP-gfp* (*Foxp3^LSL*) knockin mice (Hu et al., 2021) to report Foxp3 transcription by Thy1.1 without producing functional Foxp3 protein (Figure 6A). Because these mice had severe autoimmune inflammation, we generated chimeric mice with WT CD45.1 and *Foxp3^LSL* CD45.2 bone marrow cells mixed at a 1:1 ratio to suppress autoreactive Te cells (Figure 6B). We isolated CD45.2⁺ *Foxp3^LSL* CD4 Tn cells from these healthy chimeric mice and induced Thy1.1-expressing “wannabe” iT_{reg} cells in T_{reg}-induction media with or without supplemented ASC. Lack of Foxp3 protein appeared to be dispensable for Thy1.1 induction (Figure S6A). ASC treatment led to a mild increase of GFP-Foxp3 fusion protein in WT iT_{reg} cells and of Thy1.1 protein in wannabe iT_{reg} cells (Figures S6B and S6C).

We then assessed the stability of Thy1.1 expression *in vitro*. More than 55% of control iT_{reg} cells and more than 80% of wannabe iT_{reg} cells failed to maintain Foxp3 or Thy1.1 expression, respectively (Figure 6C), suggesting a role of the Foxp3 feedforward loop in sustaining Foxp3 transcription likely through a DNA demethylation and CNS2-independent mechanism. Among ASC-treated cells, Foxp3⁺ or Thy1.1⁺ cells were drastically increased. Consistently, ASC treatment significantly enhanced nascent Thy1.1 transcripts (Figure 6D).

To examine the stability of Thy1.1 expression *in vivo*, we sorted wannabe iT_{reg} cells and cotransferred them with CD45.1 Tn and nT_{reg} cells into *Rag1^{-/-}* mice (Figure 6E). Two weeks later, approximately 20% of mock-treated and 80% of ASC-treated wannabe iT_{reg} cells maintained Thy1.1 expression (Figures 6F and 6G). To test the stability of Thy1.1 expression in wannabe T_{reg} cells developed *in vivo*, we sorted nT_{reg} cells from

male *Foxp3^{gfp}* mice and CD4⁺Thy1.1⁺ wannabe T_{reg} cells from male *Foxp3^{LSL}* mice and cotransferred them with CD45.1 CD4 Tn and nT_{reg} cells into *Rag1^{-/-}* mice (Figure 6H). Two weeks later, approximately 90% of nT_{reg} cells maintained Foxp3 expression and 70%–80% of wannabe T_{reg} cells remained Thy1.1⁺ (Figure 6I). These results indicate that the Foxp3 feedforward regulation is a minor contributor to Tet-induced stable Foxp3 transcription. However, an absence of Foxp3 protein reduced CD25 and CTLA-4 expression in a cell-intrinsic manner (Figures 6J and 6K). Lower levels of CD25 may contribute to decreased wannabe T_{reg} cell numbers (Figure S6D).

Therefore, Stat5 and Foxp3 binding at CNS2 may play only a minor role, if any, in stabilizing Foxp3 transcription in iT_{reg} cells upon Tet-induced DNA demethylation.

Multiple pathways regulate the stability of Foxp3 expression in fully differentiated iT_{reg} cells

Previous studies identified several nuclear factors or pathways in the maintenance of Foxp3 expression, including Foxo1, Ikzf1, Runx/CBFβ, Smarcd1, and Usp22 (Agnihotri et al., 2017; Cortez et al., 2020; Kerdiles et al., 2010; Loo et al., 2020; Ouyang et al., 2010; Rudra et al., 2009). We then tested whether these factors contribute to stable Foxp3 expression in ASC-treated iT_{reg} cells. Using the CRISPR approach (Figure 7A) (Platt et al., 2014), we found that, as expected, knockdown of these factors impaired the stability of Foxp3 expression in mock-treated iT_{reg} cells (Figures 7B and 7C). Remarkably, ASC treatment always demonstrated an additive effect on the stability and levels of Foxp3 expression, suggesting multiple independent pathways governing the stability of Foxp3 expression. The Tet/ASC-CNS2 axis likely stabilizes Foxp3 transcription through several downstream factors or pathways that act in a partially redundant manner.

In summary, we modeled T_{reg} cell induction and lineage commitment with the differentiation of CD4 Tn cells to iT_{reg} cells to understand the transcriptional drivers of Foxp3 expression during this process (Figure 7D). We found that histone acetylation signal via BRD proteins targeted by JQ1 was required for the initiation of Foxp3 induction in *cis*; upon induction, it sustained Foxp3 expression in *trans* by maintaining the expression of Foxp3 positive regulators; and subsequently Tet/ASC-induced DNA demethylation of *Foxp3* enhancer CNS2 obviated the need for this histone acetylation signal in sustaining Foxp3 transcription. These distinct epigenetic mechanisms depict sequential mechanistic switches governing iT_{reg} cell lineage commitment.

DISCUSSION

Although stabilization of Foxp3 expression in iT_{reg} cells upon ASC treatment is mainly mediated by CNS2, CNS2 deficiency only slightly impairs the stability of Foxp3 expression in nT_{reg} cells (Feng et al., 2014; Li et al., 2014; Zheng et al., 2010). CNS0 plays a complementary role in maintaining Foxp3 expression in CNS2-deficient nT_{reg} cells (Zong et al., 2021) but not in ASC-treated CNS2-deficient iT_{reg} cells. Undetermined differences of epigenetic programs in ASC-treated iT_{reg} cells likely fail to activate CNS0 to sustain Foxp3 expression in the absence of CNS2.

The distinct roles of histone acetylation signal via BRD proteins targeted by JQ1 in Foxp3 induction and maintenance reflect the mechanistic switches governing iT_{reg} cell differentiation. This mechanism can also be targeted to enhance or restrict T_{reg} cell development *in vivo*. For example, short chain fatty acid butyrate enhances histone acetylation by inhibiting HDAC activity, thus promoting T_{reg} cell development (Arpaia et al., 2013; Furusawa et al., 2013).

Consistent with a recent report (Yue et al., 2021), we found that ASC treatment increases the chromatin accessibility of CNS2 in iT_{reg} cells, accompanied by markedly enhanced Stat5 and Foxp3 binding. Although similar results have been shown by *in vitro* binding and reporter assays (Kim and Leonard, 2007; Polansky et al., 2010; Zheng et al., 2010), in the absence of native genomic context, such data did not reveal the function of individual factors bound at hypomethylated CNS2. We found that demethylation of CNS2 induces a drastic switch of the regulatory modes of Foxp3 transcription. Counterintuitively, Stat5 and Foxp3 binding at hypomethylated CNS2 appears to play only a minor role, if any, in stabilizing Foxp3 expression.

Demethylation of 12 CpG sites in CNS2 during iT_{reg} cell development likely creates “parallel” regulatory circuits such that loss of the binding of individual factors would generate a minor impact on the stability of Foxp3 transcription. Our CRISPR knockdown experiment suggests that several nuclear factors reported for the maintenance of Foxp3 expression might act in parallel to the Tet/ASC-DNA demethylation pathway. These data together with the coordinative function between CNS0 and CNS2 (Zong et al., 2021) argue that Foxp3 expression in mature T_{reg} cells is controlled by multiple factors or pathways including DNA demethylation-dependent and DNA demethylation-independent mechanisms to reinforce stable Foxp3 expression and T_{reg} cell fate. Notably, 5-hydroxymethylcytosine (hmC) as an intermediate step of Tet/ASC-induced DNA demethylation has been captured in a broad range of the *Foxp3* locus during T_{reg} fate determination (Yue et al., 2021; Yue et al., 2016). Future work is needed to reveal its dynamic regulation and potential function in Foxp3 expression.

Limitations of the study

Our study heavily relies on pharmacological inhibitors. Although their target specificities have been proven, genetic approaches are needed to confirm our results. JQ1 blocks only a subset of histone acetylation readers. Future experiments are required to determine whether other histone acetylation readers also play important roles in Foxp3 induction and maintenance. Because of the considerable differences between ASC-treated iT_{reg} and nT_{reg} cells, the epigenetic mechanisms revealed in this study should be verified with nT_{reg} cells during their differentiation *in vivo*.

STAR★METHODS

RESOURCE AVAILABILITY

Lead contact—Further information and requests for resources and reagents should be directed to and will be fulfilled by the Lead Contact, Yongqiang Feng (yong.feng@stjude.org).

Materials availability—The materials are listed in the Key resources table, and are available from the Lead Contact.

Data and code availability

- The sequencing data have been deposited at <https://www.ncbi.nlm.nih.gov/geo/> with accession number GSE146250.
- This paper does not report original code.
- Any additional information required to reanalyze the data reported in this paper is available from the lead contact upon request.

EXPERIMENTAL MODEL AND SUBJECT DETAILS

Mice—All animal experiments were approved by St. Jude Children’s Research Hospital’s Institutional Animal Care and Use Committee (approval number 612). All mice were maintained and bred in a specific pathogen-free facility. Six- to twelve-week-old male and female mice were used for T_{reg} experiments. Because the *Foxp3* gene is on the X chromosome, which undergoes random inactivation in females, male mice were used for epigenetic experiments, including whole-genome bisulfite sequencing, chromatin accessibility, ChIP, and Cut&Run assays. *Foxp3^{3gfp}*, *Foxp3^{CNS2-gfp}*, *Foxp3^{CNS0-gfp}*, and *Tet1^{fl/fl} Tet2^{fl/fl} Tet3^{fl/fl} (Tet1-3^{fl/fl})* mice were described previously (Dikiy et al., 2021; Fontenot et al., 2005; Herzog et al., 2017; Zheng et al., 2010). *Foxp3^{loxP-Thy1.1-Stop-loxP-gfp}* (*Foxp3^{L^{SL}}*) mice were generated by inserting the loxP-Thy1.1-Stop-loxP-gfp cassette into a *Foxp3* intron before the coding sequence (Hu et al., 2021). *Rosa^{Cas9}* and *Foxp3^{3gfp}* mice were bred to generate *Rosa^{Cas9/+} Foxp3^{3gfp}* mice.

METHOD DETAILS

T cell isolation and culture—CD4 T cells from the lymph nodes and spleens were enriched via EasySep Mouse CD4 T Cell Isolation Kits. CD4 naive T cells (Tn, CD4⁺CD25⁻CD44⁻CD62L^{hi}) and nT_{reg} cells (CD4⁺ GFP⁺) cells were further sorted by FACS. T cells were cultured at 37°C, 5% CO₂ in complete RPMI1640 medium (RPMI1640 supplemented with 10% fetal bovine serum [FBS], 2 mM L-glutamine, 1 mM sodium pyruvate, 1% non-essential amino acid, 10 mM HEPES, 20 μM 2-mercaptoethanol, 100 U/mL penicillin, and 100 mg/mL streptomycin) and indicated cytokines and compounds. To trace cell division, cells were labeled with CellTrace Violet according to the manufacturer’s protocols.

T_{reg} cell induction and stability assays—Induction of T_{reg} or wannabe T_{reg} cell differentiation *in vitro* was conducted according to published protocols (Feng et al., 2015);

water was immediately added to perform transposition at 42°C for 40 min. DNA was purified by using the NucleoSpin Gel and PCR Clean-up kit (MACHEREY-NAGEL). The transposed DNA was amplified by PCR for 10–12 cycles by using the Nextera DNA Library Preparation Kit and Nextera XT Indexing Kit (Illumina). The library DNA within the 150- to 500-bp range was enriched by AMPure XP beads, quantified by NEBNext Library Quant Kit, and sequenced with paired-end 100 cycles on a HiSeq 4000 sequencer (Illumina).

ChIP qPCR and sequencing—CD4 Tn cells from *Foxp3^{gfp}*, *Foxp3^{CNS2-gfp}*, or *Foxp3^{CNS0-gfp}* male mice were induced to become iT_{reg} or Th0 cells in the presence or absence of 0.25 mM ascorbic acid-2-phosphate. The nT_{reg} cells from *Foxp3^{gfp}* male mice were FACS sorted and expanded *in vitro* for 5 d by using Dynabeads Mouse T-Activator CD3/CD28 in the presence of 500 U/mL recombinant IL-2. To perform Stat5 ChIP, iT_{reg} or nT_{reg} cells were starved for 3 h in complete RPMI1640 without cytokines. Cells were then restimulated with 500 U/mL IL-2 for 30 min. For Stat5, Foxp3, and RNA polymerase II ChIP, a two-step protocol was used to fix the cells as we previously described (Feng et al., 2014). In brief, cells were resuspended at 5×10^6 cells/mL in 1 mM MgCl₂/PBS and treated with 2 mM DSG cross-linker at room temperature for 30 min on a rotator. Cells were then washed twice with PBS and fixed with 1% formaldehyde at room temperature for 5 min. Fixation was quenched by adding 125 mM glycine. Cells were washed once with ice-cold PBS, aliquoted, and either frozen at –80°C or immediately processed by downstream reactions. Chromatin sonication was performed by using the truChIP Chromatin Shearing Kit (Covaris) with Focused-Ultrasonicator M220 (Corvaris) following the manufacturer’s instructions. 10×10^6 cells were used for each ChIP. Chromatin was sheared to 400–800 bp; 10% of samples were aliquoted as input control. In each ChIP reaction, 5 µL of rabbit anti-Stat5, 10 µL of rabbit anti-Foxp3, 4 µL of rabbit anti-RNA polymerase II antibodies, or control rabbit IgG were added to the lysis/binding buffer (50 mM HEPES pH 8.0, 1 mM EDTA, 1% Triton X-100, 0.1% sodium deoxycholate, 0.1% SDS, 140 mM NaCl, 1 mM PMSF, and protease inhibitor cocktail) to precipitate the chromatin. After an overnight incubation, protein A and protein G magnetic beads were added to capture the antibody-chromatin complexes. Next, beads were washed according to our published protocols (Feng et al., 2014). To release the DNA, ChIP samples were treated with proteinase K, followed by phenol: chloroform:isoamyl alcohol extraction and 2-propanol precipitation in the presence of GlycoBlue Coprecipitant. DNA pellets were dissolved in 1 × TE buffer (10 mM Tris HCl pH 8.0, 1 mM EDTA) for qPCR or deep sequencing.

For histone H3K27ac ChIP, CD4 Tn cells from *Foxp3^{gfp}* or *Foxp3^{CNS0-gfp}* male mice were induced to iT_{reg} or Th0 cells in the presence or absence of 0.25 mM ascorbic acid-2-phosphate for 4 d or cultured in T_{reg}-induction medium for 24 h with or without JQ1 or C646. iT_{reg} cells were FACS sorted by GFP expression at d 4 of induction, resuspended at 5×10^6 cells/mL in PBS, fixed with 1% formaldehyde at room temperature for 5 min, and then quenched by 125 mM glycine. 2×10^6 cells were used for each ChIP. Chromatin was sheared to 200–500 bp, and 1 µL of rabbit anti-H3K27ac antibody was used for each ChIP.

To quantify the precipitated DNA, qPCR was performed with locus- or region-specific primers, PowerUp SYBR Green Master Mix, and the CFX384 Real Time PCR System (Bio-Rad). Relative enrichment of the targets was calculated by normalizing the signals of

the precipitated DNA to those of the input samples. To perform ChIP-Seq, libraries were prepared with precipitated DNA by using the KAPA Hyper Prep Kits. The library DNA was enriched by size selection with AMPure XP beads and quantified by using the NEBNext Library Quant Kit. Indexed samples were pooled together for 100 cycles of paired end sequencing on a HiSeq 4000 or HiSeq 2500 system (Illumina). More than 40 million reads per sample were sequenced for downstream analysis.

Quantification of nascent RNA—Cells were labeled with 0.5 mM ethynyl uridine for 45 min (2.5×10^6 cells/mL culture medium) before being lysed with TRIzol reagent according to the manufacturer's protocol. Total RNA was isolated via chloroform separation and 2-propanol precipitation; 1 μ g RNA was then used for the click reaction followed by a purification with Dynabeads MyOne Streptavidin T1 beads according to the manufacturer's protocol (Click-iT Nascent RNA Capture Kits). Enriched nascent RNA was immediately used as a template to generate cDNA with the SuperScript VILO cDNA Synthesis Kit. Quantification of Foxp3 transcripts was conducted with specific primers on the CFX384 Real Time PCR System.

Quantification of total mRNA—Live cells were sorted after induction or stability assays and lysed with TRIzol reagent according to the manufacturer's protocol. Total RNA was isolated by 2-propanol precipitation. 1 μ g RNA was then used to generate cDNA with the SuperScript VILO cDNA Synthesis Kits. Quantification of Foxp3 transcripts was conducted with specific primers on the CFX384 Real Time PCR System.

SLAM Sequencing—SLAM-seq was performed according to published protocols (Muhar et al., 2018). Briefly, CD4 Tn cells isolated from *Foxp3^{gfp}* male mice were induced to iT_{reg} cells in the presence or absence of 0.25 mM ascorbic acid-2-phosphate. After induction, iT_{reg} cells were FACS sorted by GFP expression and reseeded onto 12-well plates precoated with anti-CD3 and anti-CD28 antibodies (1 μ g/mL in PBS) at 2×10^6 cells per well with complete RPMI supplemented with 100 U/mL IL-2, 5 μ M JQ1, or DMSO. 1 h later, 100 μ M 4-thiouridine (4sU) was added to culture medium for 4 h to label newly synthesized RNA. Cells were then harvested and lysed by TRIzol reagent to isolate total RNA according to the manufacturer's protocols. 5 μ g of total RNA from each sample was used to purify 4sU-labeled RNA. Sequencing libraries were then prepared and sequenced on the NovaSeq platform (Illumina).

Mixed bone marrow chimeras—Mixed bone marrow chimeric mice were generated as we previously described (Zong et al., 2021). Briefly, recipient mice (CD45.1⁺CD45.2⁺) were lethally irradiated (9.5 Gy) 24 h before intravenous injection of 5×10^6 to 10×10^6 bone marrow cells from CD45.1 WT and CD45.2 *Foxp3^{LSL}* mice mixed at a 1:1 ratio. After bone marrow transfer, the recipient mice were administered neomycin (2 mg/mL) in drinking water for 3 weeks and euthanized for CD4 T cell preparations 8–10 weeks later.

Cut&Run Sequencing—Viable iT_{reg} cells were sorted by *Foxp3^{gfp}* reporter expression after induction. Cut&Run was performed as described (Skene and Henikoff, 2017). Briefly, 1×10^6 iT_{reg} cells were first attached to Concanavalin A (ConA)-coated magnetic beads, permeabilized with digitonin-wash buffer (20 mM HEPES, pH7.5, 150 mM NaCl, 0.5 mM

spermidine, 0.01% digitonin, and protease inhibitors), and then incubated with antibody (1:100 H3K27ac) for 2 h at 4°C on a rotator. The beads-cell mixture was washed thrice with digitonin-wash buffer, resuspended in 200 μ L of protein A-MNase, and incubated for 1 h at 4°C on a rotator. After 3 rounds of washing, beads were resuspended in 150 μ L of digitonin-wash buffer and chilled in an ice-water bath for 5 min; 3 μ L of 100 mM CaCl₂ was added into the tubes with gentle vortexing, and the beads were incubated in an ice-water bath for 30 min. Next, 150 μ L of 2 \times STOP buffer (170 mM NaCl, 20 mM EDTA, 20 mM EGTA, 0.05% digitonin, 20 mg/mL GlycoBlue, 25 mg/mL RNase A) was added and incubated at 37°C for 30 min. After clarification on a magnet stand, supernatant was transferred to a fresh tube for phenol:chloroform extraction and ethanol precipitation. A library was prepared by using KAPA Hyper Prep Kits, and 5 ng DNA was loaded for high-throughput sequencing.

Retroviral vectors—The retroviral backbone pSIR-DsRed-Express2 were purchased from Addgene (Fujita and Fujii, 2014). To facilitate sgRNA cloning, we removed 3 BbsI sites using QuikChange Lightning Multi Site-Directed Mutagenesis Kit (Agilent Technologies). Next, we inserted the U6 promoter-BbsI-sgRNA-BbsI cassette into the modified vector backbone between HindIII and EcoRI sites. The resulting pSIR-DsRed (BbsI) vector was validated by Sanger sequencing. We also generated pSIR-Thy1.1 (BbsI) vector by changing the reporter gene. These modified retroviral vectors enable direct cloning of sgRNA coding sequences with 2 BbsI restriction sites according to standard protocols. To clone the control or gene-specific sgRNAs into pSIR-Thy1.1 or pSIR-DsRed, 2 complementary strands of DNA oligoes were synthesized, annealed, and ligated to the BbsI-digested vector backbone with T4 DNA ligase. The inserts were confirmed by Sanger sequencing.

Retroviral packaging and transduction—Retroviral packing and transduction of mouse primary T cells were conducted according to our published protocols with minor modifications (Zong et al., 2021). Platinum-E (Plat-E) cells were used to package the retrovirus. These cells were cultured in DMEM supplemented with 10% fetal bovine serum (FBS), 10 mM HEPES, 100 U/mL penicillin, and 100 mg/mL streptomycin. In particular, 1 μ g/mL puromycin and 10 μ g/mL blasticidin were added into the culture media to maintain Plat-E cells according to the manufacturer's manual. 24 h before transfection, cells were seeded on new dishes in media without puromycin and blasticidin. sgRNA-expressing plasmid and pCl-Eco were cotransfected into these cells with TransIT-293 Transfection Reagent. 2–3 d after transfection, viral supernatant was collected and filtered with 0.45 μ m syringe filters, aliquoted, and stored at –80°C. A similar protocol was used to prepare control and Cre-expressing retrovirus with pMigR1-IRES-Thy1.1 or pMigR1-Cre-IRES-Thy1.1 plasmids, respectively.

Retrovirus titration and transduction—Titers of retroviral preps were assessed to ensure proper transduction efficiency. Specifically, 1×10^5 Tn cells were seeded on one well of 96-well plates precoated with anti-CD3 and anti-CD28 antibodies (1 μ g/mL each in PBS) to induce T_{reg} cell differentiation with recombinant human IL-2 (100 U/mL) and recombinant human TGF- β (1 ng/mL). 24 h later, 10 mg/mL polybrene and titrated amounts of viral preps were added. Cells were centrifuged at 1,200 g, 37°C for 90 min. After

transduction, culture medium was changed to fresh complete RPMI1640 supplemented with new IL-2 and TGF- β . 3 d later, cells were stained and analyzed for Thy1.1 expression by flow cytometry to determine the transduction efficiency and viral titers.

To examine the factors controlling Foxp3 expression after Tet-induced DNA demethylation, CD4 Tn cells sorted from *Rosa^{Cas9/+} Foxp3^{gfp}* mice were cultured in 6-well plates precoated with anti-CD3 and anti-CD28 antibodies at 1×10^6 cells per well in T_{reg}-induction medium supplemented with 0.25 mM ascorbic acid-2-phosphate. After 3 d of culture, cells were transduced with sgRNA-expressing retrovirus. To assay the stability of Foxp3 expression, cells were collected and reseeded into aCD3/aCD28 precoated 96-well plate with complete RPMI1640 supplemented with 100 U/mL recombinant human IL-2 for 4 d. Cells were then harvested, stained, and analyzed by flow cytometers.

QUANTIFICATION AND STATISTICAL ANALYSIS

Bisulfite sequencing—Bisulfite sequencing data were aligned to mouse genome mm9 by using BSMAP2.74 (Xi and Li, 2009). The methylation ratio for each CpG site was extracted by methratio.py from BSMAP2.74 and then converted to bw file for visualization. The M values for the 3,000 most variable CpG sites were used for hierarchical clustering and PCA analyses. M value = \log_2 (C count/T count) at a CpG site (an offset value of 0.5 was added).

ATAC sequencing—Paired-end reads of 100 bp were trimmed by cutadapt (version 1.9, paired-end mode, default parameter with “-m 25 -O 6”) (Martin, 2011) and aligned to mouse genome mm9 (MGSCv37 from Sanger) by BWA (version 0.7.12-r1039, default parameter) (Li and Durbin, 2009). Duplicate reads were marked by biobambam2 (version v2.0.87) (Tischler and Leonard, 2014); non-duplicate, properly paired reads were kept by samtools (parameter “-q 1 -F 1804” version 1.2) (Li et al., 2009). To adjust Tn5 shift, reads were offset by +4 bp for the sense strand and -5 bp for the antisense strand. We used fragment size to separate reads into nucleosome-free, mononucleosome, dinucleosome, and trinucleosome groups as described (Buenrostro et al., 2013) and generated bw files by using the center 80 bp of fragments and scale to 20 million nucleosome-free reads. Two replicates were merged to enhance peak calling by MACS2 (version 2.1.1.20160309 default parameters with “-extsize 200 -nomodel”) (Zhang et al., 2008). All the important nucleosome-free regions were considered to have been called if a sample had more than 15 million nucleosome-free reads after merging. To ensure reproducibility, we first merged peaks from different cell types to create a set of reference chromatin-accessible regions. We then used bedtools (v2.24.0) (Quinlan and Hall, 2010) to count nucleosome-free reads from each sample to overlay with the reference regions. To identify differentially accessible regions, we first normalized raw nucleosome-free reads counts by using trimmed mean of M-values (TMM) and then applied empirical Bayes statistics testing after linear fitting with voom package (R 3.23, edgeR 3.12.1, limma 3.26.9) (Law et al., 2014). A false discovery rate (FDR) adjusted *P* value < 0.05 and fold change > 2 were used as cutoff values for differentially accessible regions.

ChIP sequencing—Single-end reads of 50 bp were mapped to mouse genome mm9 (MGSCv37 from Sanger) by BWA (version 0.7.12-r1039, default parameter) (Li and

Durbin, 2009). Duplicate reads were marked with biobambam2 (version v2.0.87) (Tischler and Leonard, 2014); non-duplicate reads were kept by samtools (parameter “-q 1 -F 1024” version 1.2) (Li et al., 2009). We followed ENCODE guidelines to assess the quality of our data as previously described (Yang et al., 2019). Next, we extended reads to fragment size (detected by SPP v1.1) (Kharchenko et al., 2008) and generated bw tracks (normalized to 10 million uniquely mapped reads) for visualization. We used MACS2 (version 2.1.1.20160309, parameters “-nomodel-extsize fragment size”) to call peaks. To assure reproducibility, we finalized the peaks for each group if they were called with a stringent cutoff value (FDR-adjusted *P value* < 0.05 in MACS2) in one sample and at least called with a lower cutoff value (FDR-corrected *P value* < 0.5 in MACS2) in the other. Peaks were further merged between groups. Reads were extended to fragment size for each sample via bedtools (v2.24.0) (Quinlan and Hall, 2010). We used correlation plots to assess the reproducibility among replicates. After TMM normalization, we used empirical Bayes statistics testing after linear fitting from voom package (R 3.23, edgeR 3.12.1, limma 3.26.9) (Law et al., 2014) to identify differential binding sites. FDR-adjusted *P value* < 0.05 and fold change > 2 were used as cutoff values.

Cut&Run sequencing—After adaptor trimming by cutadapt (version 1.9, paired-end mode, default parameter with “-m 25 -O 6”) (Martin, 2011), 50-bp paired-end reads were mapped to mouse genome mm9 (MGSCv37 from Sanger) by using BWA (version 0.7.12-r1039, default parameter) (Li and Durbin, 2009). Duplicate reads were marked with biobambam2 (version v2.0.87) (Tischler and Leonard, 2014); non-duplicate reads were kept by samtools (parameter “-q 1 -F 1804” version 1.2) (Li et al., 2009). At least 5 million reads per sample were used for further analysis, as suggested in published research (Skene et al., 2018). We generated bw files using the center 80 bp of fragments smaller than 2000 bp and normalizing the reads counts to 10 million fragments.

SLAM sequencing—Single-end reads of 100 bp were first trimmed by cutadapt (version 1.9, default parameter with “-m 25 -O 6”) (Martin, 2011) and then aligned to mouse genome mm9 (MGSCv37 from Sanger) by SLAMDUNK (version 0.4.0, parameters “-5 12 -n 100 -c 2 -mv 0.2 -m -rl 100”) (Neumann et al., 2019). 3'UTR bed files from Gencode vM17 (liftOver from mm9) (Harrow et al., 2012) were used for reads counting and gene-based counting (SLAMDUNK collapse function). All samples achieved more than 100 million reads (median 120 million) and at least 98.4% mapping rate. Quality control results from SLAMDUNK (alleyoop function, all default parameters except “-mq 2” for rates subfunction) were comparable to those from published SLAM-seq data (Muhar et al., 2018).

We took the results table from SLAMDUNK and first filtered genes that required at least 10 “readCount,” 2 “tcReadCount,” and counts per million (CPM) > 1. For each comparison, we performed two differential expression analyses using two normalization methods. For nascent RNA analysis (new mRNA), we normalized nascent RNA (“tcReadCount”) with trimmed mean of M-values normalization method (TMM). For normalized nascent RNA analysis (normalized new mRNA), we normalized nascent RNA with total “readCount.” We

then applied Empirical Bayes Statistics test to “tcReadCount” after linear fitting from voom package (R 3.23, edgeR 3.12.1, limma 3.26.9) (Law et al., 2014).

STATISTICAL ANALYSIS

Statistical tests were performed using GraphPad Prism (GraphPad Software) or the R statistical environment. For data with a small sample size, a robust nonparametric Mann-Whitney test was used; otherwise, an unpaired t test was applied. All the statistical details can be found in the figure legends. ns, not significant. * $p < 0.05$; ** $p < 0.01$; *** $p < 0.001$; and **** $p < 0.0001$.

Supplementary Material

Refer to Web version on PubMed Central for supplementary material.

ACKNOWLEDGMENTS

We thank Alexander Rudensky (Memorial Sloan Kettering Cancer Center, New York, NY) for providing the mouse strains, Jaeki Min and Zoran Rankovic (St. Jude Children’s Research Hospital, Memphis, TN) for providing epigenetic inhibitors, and Cherise Guess (St. Jude Children’s Research Hospital, Memphis, TN) for editing the manuscript. X.Z. was supported by a Special Postdoctoral Fellowship of the Academic Programs Office of St. Jude Children’s Research Hospital. This study was supported by the American Lebanese Syrian Associated Charities and National Institutes of Health grants R01 AI153138 and R21 AI146614 (Y. Feng) and cancer center support grant P30 CA021765 (St. Jude Children’s Research Hospital). The content is solely the responsibility of the authors and does not necessarily represent the official views of the National Institutes of Health.

REFERENCES

- Agnihotri P, Robertson NM, Umetsu SE, Arakcheeva K, and Winandy S (2017). Lack of Ikaros cripples expression of Foxo1 and its targets in naive T cells. *Immunology* 152, 494–506. [PubMed: 28670688]
- Arpaia N, Campbell C, Fan X, Dikiy S, van der Veecken J, deRoos P, Liu H, Cross JR, Pfeffer K, Coffey PJ, and Rudensky AY (2013). Metabolites produced by commensal bacteria promote peripheral regulatory T-cell generation. *Nature* 504, 451–455. [PubMed: 24226773]
- Brunkow ME, Jeffery EW, Hjerrild KA, Paepers B, Clark LB, Yasayko SA, Wilkinson JE, Galas D, Ziegler SF, and Ramsdell F (2001). Disruption of a new forkhead/winged-helix protein, scurfy, results in the fatal lymphoproliferative disorder of the scurfy mouse. *Nat. Genet* 27, 68–73. [PubMed: 11138001]
- Buenrostro JD, Giresi PG, Zaba LC, Chang HY, and Greenleaf WJ (2013). Transposition of native chromatin for fast and sensitive epigenomic profiling of open chromatin, DNA-binding proteins and nucleosome position. *Nat. Methods* 10, 1213–1218. [PubMed: 24097267]
- Buenrostro JD, Wu B, Chang HY, and Greenleaf WJ (2015). ATAC-seq: A Method for Assaying Chromatin Accessibility Genome-Wide. *Current protocols in molecular biology*. 109, Published online January 5, 2015. 10.1002/0471142727.mb2129s109.
- Cortez JT, Montauti E, Shifrut E, Gatchalian J, Zhang Y, Shaked O, Xu Y, Roth TL, Simeonov DR, Zhang Y, et al. (2020). CRISPR screen in regulatory T cells reveals modulators of Foxp3. *Nature* 582, 416–420. [PubMed: 32499641]
- Dikiy S, Li J, Bai L, Jiang M, Janke L, Zong X, Hao X, Hoyos B, Wang ZM, Xu B, et al. (2021). A distal Foxp3 enhancer enables interleukin-2 dependent thymic Treg cell lineage commitment for robust immune tolerance. *Immunity* 54, 931–946.e11. [PubMed: 33838102]
- Feng Y, Arvey A, Chinen T, van der Veecken J, Gasteiger G, and Rudensky AY (2014). Control of the inheritance of regulatory T cell identity by a cis element in the Foxp3 locus. *Cell* 158, 749–763. [PubMed: 25126783]

- Feng Y, van der Veeke J, Shugay M, Putintseva EV, Osmanbeyoglu HU, Dikiy S, Hoyos BE, Moltedo B, Hemmers S, Treuting P, et al. (2015). A mechanism for expansion of regulatory T-cell repertoire and its role in self-tolerance. *Nature* 528, 132–136. [PubMed: 26605529]
- Fontenot JD, Gavin MA, and Rudensky AY (2003). Foxp3 programs the development and function of CD4+CD25+ regulatory T cells. *Nat. Immunol* 4, 330–336. [PubMed: 12612578]
- Fontenot JD, Rasmussen JP, Williams LM, Dooley JL, Farr AG, and Rudensky AY (2005). Regulatory T cell lineage specification by the forkhead transcription factor foxp3. *Immunity* 22, 329–341. [PubMed: 15780990]
- Fujisawa T, and Filippakopoulos P (2017). Functions of bromodomain-containing proteins and their roles in homeostasis and cancer. *Nat. Rev. Mol. Cell Biol* 18, 246–262. [PubMed: 28053347]
- Fujita T, and Fujii H (2014). Identification of proteins associated with an IFN γ -responsive promoter by a retroviral expression system for enChIP using CRISPR. *PLoS ONE* 9, e103084. [PubMed: 25051498]
- Furusawa Y, Obata Y, Fukuda S, Endo TA, Nakato G, Takahashi D, Nakanishi Y, Uetake C, Kato K, Kato T, et al. (2013). Commensal microbe-derived butyrate induces the differentiation of colonic regulatory T cells. *Nature* 504, 446–450. [PubMed: 24226770]
- Gavin M, and Rudensky A (2003). Control of immune homeostasis by naturally arising regulatory CD4+ T cells. *Curr. Opin. Immunol* 15, 690–696. [PubMed: 14630204]
- Harrow J, Frankish A, Gonzalez JM, Tapanari E, Diekhans M, Kokocinski F, Aken BL, Barrell D, Zadissa A, Searle S, et al. (2012). GENCODE: the reference human genome annotation for The ENCODE Project. *Genome Res.* 22, 1760–1774. [PubMed: 22955987]
- Herzig Y, Nevo S, Bornstein C, Brezis MR, Ben-Hur S, Shkedy A, Eisenberg-Bord M, Levi B, Delacher M, Goldfarb Y, et al. (2017). Transcriptional programs that control expression of the autoimmune regulator gene Aire. *Nat. Immunol* 18, 161–172. [PubMed: 27941786]
- Hori S, Nomura T, and Sakaguchi S (2003). Control of regulatory T cell development by the transcription factor Foxp3. *Science* 299, 1057–1061. [PubMed: 12522256]
- Hu W, Wang ZM, Feng Y, Schizas M, Hoyos BE, van der Veeke J, Verter JG, Bou-Puerto R, and Rudensky AY (2021). Regulatory T cells function in established systemic inflammation and reverse fatal autoimmunity. *Nat. Immunol* 22, 1163–1174. [PubMed: 34426690]
- Josefowicz SZ, Wilson CB, and Rudensky AY (2009). Cutting edge: TCR stimulation is sufficient for induction of Foxp3 expression in the absence of DNA methyltransferase 1. *J. Immunol* 182, 6648–6652. [PubMed: 19454658]
- Josefowicz SZ, Lu LF, and Rudensky AY (2012). Regulatory T cells: mechanisms of differentiation and function. *Annu. Rev. Immunol* 30, 531–564. [PubMed: 22224781]
- Kawakami R, Kitagawa Y, Chen KY, Arai M, Ohara D, Nakamura Y, Yasuda K, Osaki M, Mikami N, Lareau CA, et al. (2021). Distinct Foxp3 enhancer elements coordinate development, maintenance, and function of regulatory T cells. *Immunity* 54, 947–961.e8. [PubMed: 33930308]
- Kerdiles YM, Stone EL, Beisner DR, McGargill MA, Ch'en IL, Stockmann C, Katayama CD, and Hedrick SM (2010). Foxo transcription factors control regulatory T cell development and function. *Immunity* 33, 890–904. [PubMed: 21167754]
- Kharchenko PV, Tolstorukov MY, and Park PJ (2008). Design and analysis of ChIP-seq experiments for DNA-binding proteins. *Nat. Biotechnol* 26, 1351–1359. [PubMed: 19029915]
- Kim HP, and Leonard WJ (2007). CREB/ATF-dependent T cell receptor-induced FoxP3 gene expression: a role for DNA methylation. *J. Exp. Med* 204, 1543–1551. [PubMed: 17591856]
- Kim JM, Rasmussen JP, and Rudensky AY (2007). Regulatory T cells prevent catastrophic autoimmunity throughout the lifespan of mice. *Nat. Immunol* 8, 191–197. [PubMed: 17136045]
- Law CW, Chen Y, Shi W, and Smyth GK (2014). voom: Precision weights unlock linear model analysis tools for RNA-seq read counts. *Genome Biol.* 15, R29. [PubMed: 24485249]
- Li H, and Durbin R (2009). Fast and accurate short read alignment with Burrows-Wheeler transform. *Bioinformatics* 25, 1754–1760. [PubMed: 19451168]
- Li H, Handsaker B, Wysoker A, Fennell T, Ruan J, Homer N, Marth G, Abecasis G, and Durbin R; 1000 Genome Project Data Processing Subgroup (2009). The Sequence Alignment/Map format and SAMtools. *Bioinformatics* 25, 2078–2079. [PubMed: 19505943]

- Li X, Liang Y, LeBlanc M, Benner C, and Zheng Y (2014). Function of a Foxp3 cis-element in protecting regulatory T cell identity. *Cell* 158, 734–748. [PubMed: 25126782]
- Liston A, Farr AG, Chen Z, Benoist C, Mathis D, Manley NR, and Rudensky AY (2007). Lack of Foxp3 function and expression in the thymic epithelium. *J. Exp. Med* 204, 475–480. [PubMed: 17353370]
- Liu Y, Wang L, Predina J, Han R, Beier UH, Wang L-CS, Kapoor V, Bhatti TR, Akimova T, Singhal S, et al. (2013). Inhibition of p300 impairs Foxp3+ T regulatory cell function and promotes antitumor immunity. *Nat Med*. 19, 1173–1177. [PubMed: 23955711]
- Liu Y, Wang L, Han R, Beier UH, Akimova T, Bhatti T, Xiao H, Cole PA, Brindle PK, and Hancock WW (2014). Two histone/protein acetyltransferases, CBP and p300, are indispensable for Foxp3+ T-regulatory cell development and function. *Mol. Cell. Biol* 34, 3993–4007. [PubMed: 25154413]
- Loo CS, Gatchalian J, Liang Y, Leblanc M, Xie M, Ho J, Venkatraghavan B, Hargreaves DC, and Zheng Y (2020). A Genome-wide CRISPR Screen Reveals a Role for the Non-canonical Nucleosome-Remodeling BAF Complex in Foxp3 Expression and Regulatory T Cell Function. *Immunity* 53, 143–157.e8. [PubMed: 32640256]
- Marmorstein R, and Zhou MM (2014). Writers and readers of histone acetylation: structure, mechanism, and inhibition. *Cold Spring Harb. Perspect. Biol* 6, a018762. [PubMed: 24984779]
- Martin M (2011). Cutadapt removes adapter sequences from high-throughput sequencing reads. *EMBnetjournal*. 17. 10.14806/ej.17.1.200.
- Muhar M, Ebert A, Neumann T, Umkehrer C, Jude J, Wieshofer C, Rescheneder P, Lipp JJ, Herzog VA, Reichholf B, et al. (2018). SLAM-seq defines direct gene-regulatory functions of the BRD4-MYC axis. *Science* 360, 800–805. [PubMed: 29622725]
- Nakatsukasa H, Oda M, Yin J, Chikuma S, Ito M, Koga-Iizuka M, Someya K, Kitagawa Y, Ohkura N, Sakaguchi S, et al. (2019). Loss of TET proteins in regulatory T cells promotes abnormal proliferation, Foxp3 destabilization and IL-17 expression. *Int. Immunol* 31, 335–347. [PubMed: 30726915]
- Neumann T, Herzog VA, Muhar M, von Haeseler A, Zuber J, Ameres SL, and Rescheneder P (2019). Quantification of experimentally induced nucleotide conversions in high-throughput sequencing datasets. *BMC Bioinformatics* 20, 258. [PubMed: 31109287]
- Ohkura N, and Sakaguchi S (2020). Transcriptional and epigenetic basis of Treg cell development and function: its genetic anomalies or variations in autoimmune diseases. *Cell Res*. 30, 465–474. [PubMed: 32367041]
- Ohkura N, Hamaguchi M, Morikawa H, Sugimura K, Tanaka A, Ito Y, Osaki M, Tanaka Y, Yamashita R, Nakano N, et al. (2012). T cell receptor stimulation-induced epigenetic changes and Foxp3 expression are independent and complementary events required for Treg cell development. *Immunity* 37, 785–799. [PubMed: 23123060]
- Ouyang W, Beckett O, Ma Q, Paik JH, DePinho RA, and Li MO (2010). Foxo proteins cooperatively control the differentiation of Foxp3+ regulatory T cells. *Nat. Immunol* 11, 618–627. [PubMed: 20467422]
- Platt RJ, Chen S, Zhou Y, Yim MJ, Swiech L, Kempton HR, Dahlman JE, Parnas O, Eisenhaure TM, Jovanovic M, et al. (2014). CRISPR-Cas9 knockin mice for genome editing and cancer modeling. *Cell* 159, 440–455. [PubMed: 25263330]
- Polansky JK, Schreiber L, Thelemann C, Ludwig L, Krüger M, Baum-grass R, Cording S, Floess S, Hamann A, and Huehn J (2010). Methylation matters: binding of Ets-1 to the demethylated Foxp3 gene contributes to the stabilization of Foxp3 expression in regulatory T cells. *J. Mol. Med. (Berl.)* 88, 1029–1040. [PubMed: 20574810]
- Quinlan AR, and Hall IM (2010). BEDTools: a flexible suite of utilities for comparing genomic features. *Bioinformatics* 26, 841–842. [PubMed: 20110278]
- Rubtsov YP, Niec RE, Josefowicz S, Li L, Darce J, Mathis D, Benoist C, and Rudensky AY (2010). Stability of the regulatory T cell lineage in vivo. *Science* 329, 1667–1671. [PubMed: 20929851]
- Rudensky AY (2011). Regulatory T cells and Foxp3. *Immunol. Rev* 241, 260–268. [PubMed: 21488902]

- Rudra D, Egawa T, Chong MM, Treuting P, Littman DR, and Rudensky AY (2009). Runx-CBFbeta complexes control expression of the transcription factor Foxp3 in regulatory T cells. *Nat. Immunol* 10, 1170–1177. [PubMed: 19767756]
- Samstein RM, Arvey A, Josefowicz SZ, Peng X, Reynolds A, Sandstrom R, Neph S, Sabo P, Kim JM, Liao W, et al. (2012). Foxp3 exploits a pre-existent enhancer landscape for regulatory T cell lineage specification. *Cell* 151, 153–166. [PubMed: 23021222]
- Sasidharan Nair V, Song MH, and Oh KI (2016). Vitamin C Facilitates Demethylation of the Foxp3 Enhancer in a Tet-Dependent Manner. *J. Immunol* 196, 2119–2131. [PubMed: 26826239]
- Savage PA, Klawon DEJ, and Miller CH (2020). Regulatory T Cell Development. *Annu. Rev. Immunol* 38, 421–453. [PubMed: 31990619]
- Skene PJ, and Henikoff S (2017). An efficient targeted nuclease strategy for high-resolution mapping of DNA binding sites. *eLife* 6, e21856. [PubMed: 28079019]
- Skene PJ, Henikoff JG, and Henikoff S (2018). Targeted in situ genome-wide profiling with high efficiency for low cell numbers. *Nat. Protoc* 13, 1006–1019. [PubMed: 29651053]
- Tischler G, and Leonard S (2014). biobambam: tools for read pair collation based algorithms on BAM files. *Source Code Biol. Med* 9, 13.
- Xi Y, and Li W (2009). BSMAP: whole genome bisulfite sequence MAPPING program. *BMC Bioinformatics* 10, 232. [PubMed: 19635165]
- Yang X, Xu B, Mulvey B, Evans M, Jordan S, Wang YD, Pagala V, Peng J, Fan Y, Patel A, and Peng JC (2019). Differentiation of human pluripotent stem cells into neurons or cortical organoids requires transcriptional co-regulation by UTX and 53BP1. *Nat. Neurosci* 22, 362–373. [PubMed: 30718900]
- Yue X, Trifari S, Äijö T, Tsagaratou A, Pastor WA, Zepeda-Martínez JA, Lio CW, Li X, Huang Y, Vijayanand P, et al. (2016). Control of Foxp3 stability through modulation of TET activity. *J. Exp. Med* 213, 377–397. [PubMed: 26903244]
- Yue X, Lio CJ, Samaniego-Castruita D, Li X, and Rao A (2019). Loss of TET2 and TET3 in regulatory T cells unleashes effector function. *Nat. Commun* 10, 2011. [PubMed: 31043609]
- Yue X, Samaniego-Castruita D, González-Avalos E, Li X, Barwick BG, and Rao A (2021). Whole-genome analysis of TET dioxygenase function in regulatory T cells. *EMBO Rep.* 22, e52716. [PubMed: 34288360]
- Zhang Y, Liu T, Meyer CA, Eeckhoute J, Johnson DS, Bernstein BE, Nusbaum C, Myers RM, Brown M, Li W, and Liu XS (2008). Model-based analysis of ChIP-Seq (MACS). *Genome Biol.* 9, R137. [PubMed: 18798982]
- Zheng Y, Josefowicz S, Chaudhry A, Peng XP, Forbush K, and Rudensky AY (2010). Role of conserved non-coding DNA elements in the Foxp3 gene in regulatory T-cell fate. *Nature* 463, 808–812. [PubMed: 20072126]
- Zong X, Hao X, Xu B, Crawford JC, Wright S, Li J, Zhang Y, Bai L, He M, Jiang M, et al. (2021). Foxp3 enhancers synergize to maximize regulatory T cell suppressive capacity. *J. Exp. Med* 218, e20202415. [PubMed: 34086055]

Highlights

- Promoter histone acetylation facilitates Foxp3 induction in *cis*
- Histone acetylation maintains Foxp3 transcription in *trans* before DNA demethylation
- Tet-induced DNA demethylation rewires Foxp3 transcriptional regulation in *cis*
- Histone acetylation is dispensable for stable Foxp3 transcription afterward

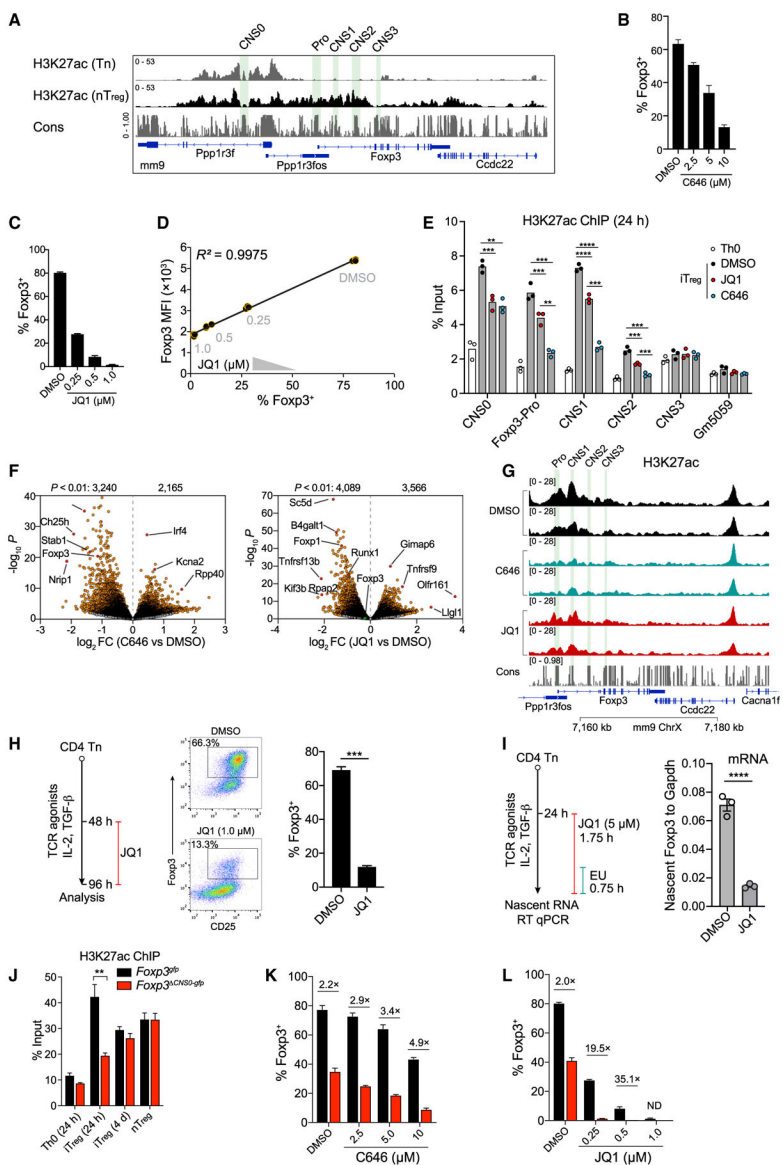


Figure 1. Histone acetylation drives Foxp3 induction efficiency and expression levels during early iTreg cell development

(A) Histone H3K27ac around the *Foxp3* locus assessed by Cut&Run-seq. Pro, promoter. Cons, DNA sequence conservation among placental mammals. Data represent 3 experiments.

(B) CD4 Tn cells were cultured in Treg-induction medium with or without C646 for 4 d before analysis of Foxp3 expression in live cells. Data show means + SEMs of triplicates and represent 3 experiments.

(C and D) JQ1 was added during iTreg cell induction and live cells were gated for analysis at d 4. MFI, median fluorescence intensity. Data show means + SEMs of triplicates and represent 3 experiments.

(E) CD4 Tn cells were cultured in Th0 or T_{reg}-induction conditions for 24 h in the presence of DMSO, JQ1 (1 μ M), or C646 (10 μ M) before analyzing H3K27ac by ChIP qPCR. Triplicates are shown. Data represent 2 experiments.

(F and G) H3K27ac ChIP-seq of cells described above (E). Numbers of genes significantly ($p < 0.01$) increased or decreased are shown (F). H3K27ac around the *Foxp3* locus is compared among samples (G). Data were pooled from 2 biological replicates. FC, fold change.

(H) JQ1 (1 μ M) was added at d 2 during iT_{reg} induction and cells were analyzed at d 4. Data show means + SEMs of triplicates and represent 2 experiments.

(I) Quantification of nascent *Foxp3* mRNA during acute JQ1 treatment. Triplicates are shown. Data represent 2 experiments.

(J) H3K27ac at the *Foxp3* promoter. Cells were cultured in Th0 or T_{reg}-induction media for 24 h or 4 d before ChIP qPCR. Data show means + SEMs of triplicates and represent 2 experiments.

(K and L) *Foxp3* induction from CD4 Tn cells in the presence of titrated C646 (K) or JQ1 (L) for 4 d. Data show means + SEMs of triplicates and represent 2 experiments.

Unpaired, two-tailed t test.

See also Figure S1.

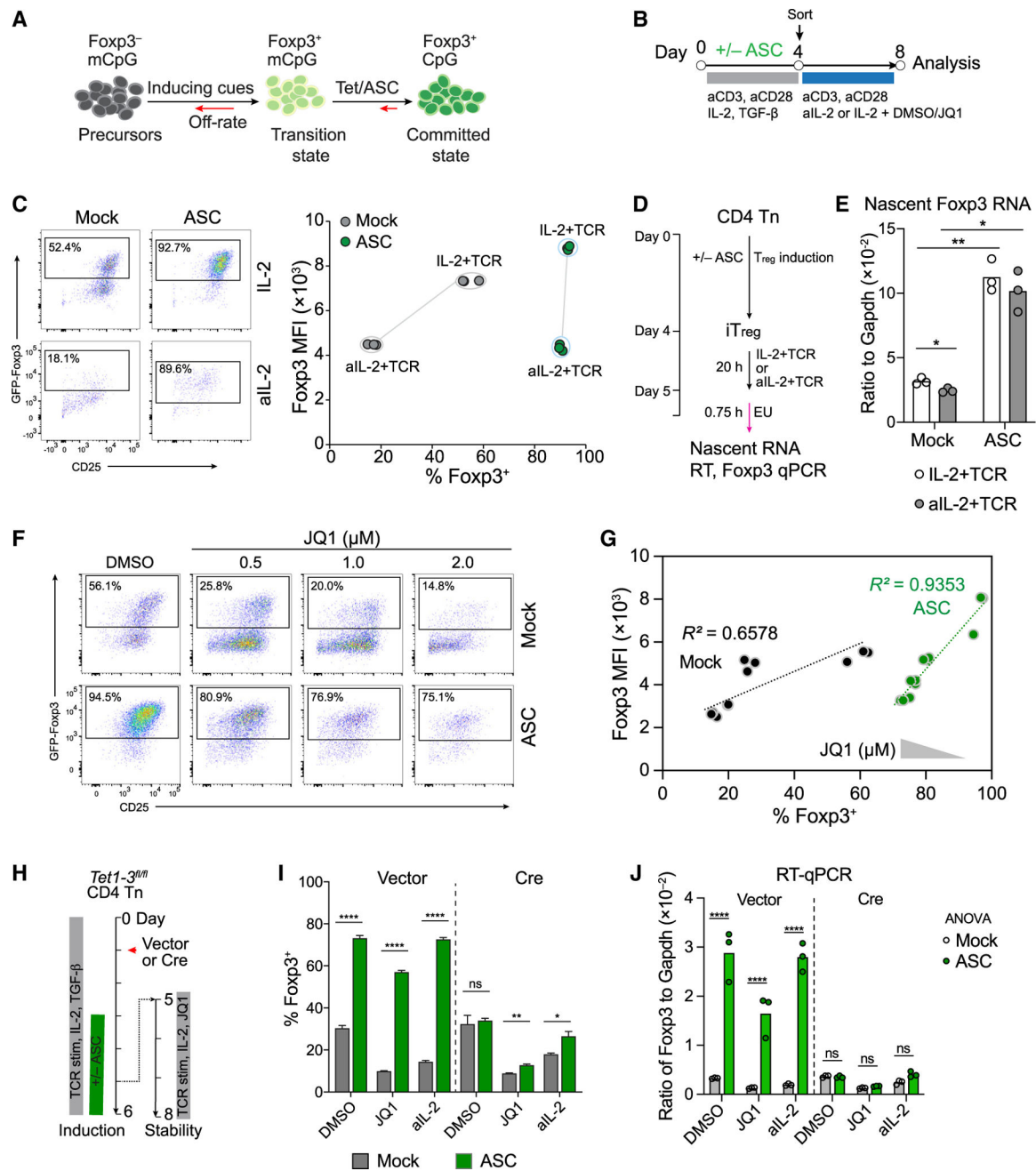


Figure 2. Histone acetylation signal via BRD proteins targeted by JQ1 is dispensable for stable Foxp3 expression in ASC-treated iT_{reg} cells

(A) Schematic processes of T_{reg} cell lineage commitment. mCpG, methylated CpG. Off rate indicates unstable Foxp3 expression.

(B) Experimental procedures for assaying the stability of Foxp3 expression in iT_{reg} cells.

(C) The stability and levels of Foxp3 expression in mock- and ASC-pretreated iT_{reg} cells. Technical replicates are shown. Data represent 2 experiments.

(D and E) Quantification of Foxp3 transcription by EU pulse labeling and RT-qPCR. Triplicates are shown. Data represent 2 experiments.

(D and E) Quantification of Foxp3 transcription by EU pulse labeling and RT-qPCR. Triplicates are shown. Data represent 2 experiments.

(D and E) Quantification of Foxp3 transcription by EU pulse labeling and RT-qPCR. Triplicates are shown. Data represent 2 experiments.

(F and G) Foxp3 expression in mock- and ASC-pretreated iT_{reg} cells grown in media containing titrated JQ1 for an additional 4 d. Data represent 3 experiments.

(H–J) CD4 Tn cells isolated from *Tet1-3^{fl/fl}* mice were cultured in T_{reg}-induction medium. Retroviral Cre was transduced at d 1 and PBS or ASC was added from d 3 to d 5. Cells were then grown in media containing DMSO (with IL-2), aIL-2, or JQ1 (with IL-2) with TCR agonists for an additional 3 d before analyzing Foxp3⁺ cells (H, I). Total live cells were also used to quantify Foxp3 and Gapdh mRNA with RT-qPCR (J). Data show means + SEMs of triplicates and represent 2 experiments.

Unpaired, two-tailed t test.

See also Figure S2.

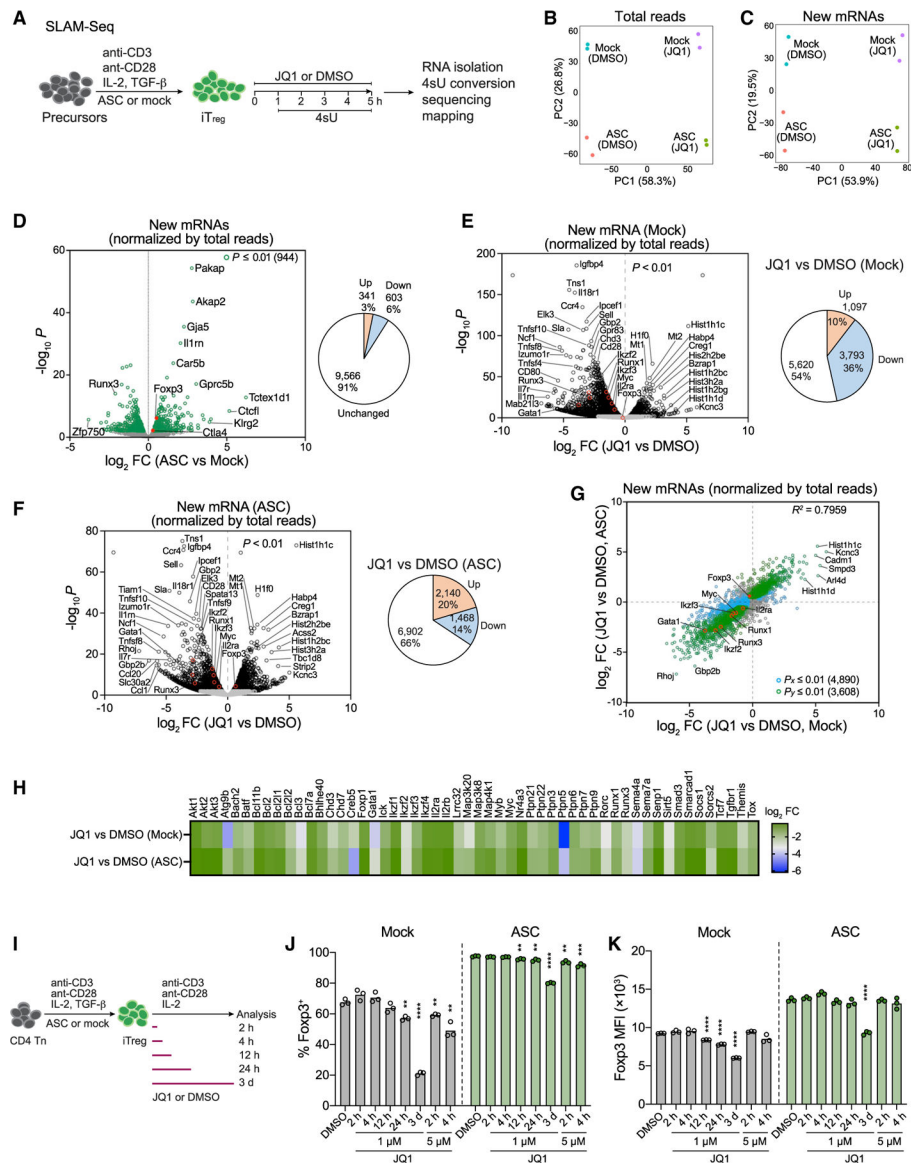


Figure 3. The role of histone acetylation via BRD proteins targeted by JQ1 in controlling Foxp3 expression in differentiated iT_{reg} cells

(A) Experimental procedures for quantifying global transcriptional activity by SLAM-seq. (B and C) Principal components analysis of total RNA (B) and 4sU-labeled new mRNA reads (C). $n = 2$ replicates. Percentages of total variations are shown in parenthesis. (D–F) Differentially expressed genes between comparison groups assessed by new RNAs. Genes significantly up- and downregulated ($p < 0.01$) are highlighted and counted by the pie charts. (G) Comparison of the changes of JQ1 versus DMSO treatment between mock- and ASC-pretreated iT_{reg} cells. Genes differentially expressed ($p < 0.01$) on the x axis are colored in blue and those on the y axis in green. (H) Select genes downregulated in JQ1- versus DMSO-treated iT_{reg} cells ($p < 0.01$). (I–K) Mock- or ASC-treated iT_{reg} cells were sorted at d 4 to assay the reversibility of Foxp3 expression upon JQ1 treatment. Cells were analyzed 3 d later (I). Live cells were gated to

quantify Foxp3⁺ cells (J) and Foxp3 MFI (K). Data represent two experiments. Unpaired, two-tailed t test.
See also Figure S3.

Author Manuscript

Author Manuscript

Author Manuscript

Author Manuscript

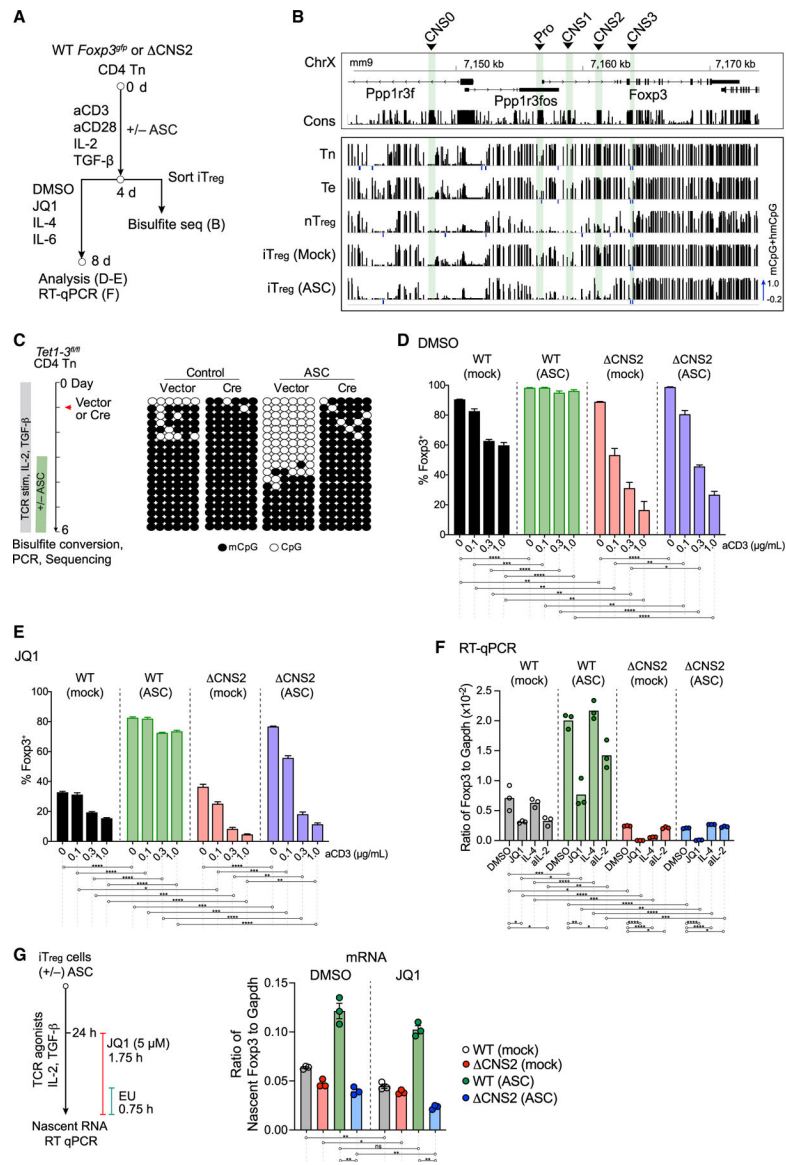


Figure 4. CNS2 is required for Tet/DNA demethylation-dependent stabilization of Foxp3 expression

(A) Experimental procedures.

(B) DNA methylation status around the *Foxp3* locus. Vertical lines represent individual CpG sites and methylation levels (mCpG and hmCpG combined) range from 0 (unmethylated) to 1 (methylated). Data were merged from 2 biological replicates. Regions covered by < 5 reads are marked as -0.2.

(C) Methylation status at select CpG sites of CNS2 quantified by bisulfite PCR-seq in iTreg cells after acute deletion of *Tet1-3* followed by mock or ASC treatment. Rows of dots represent individual DNA molecules.

(D and E) Stability of Foxp3 expression in WT *Foxp3^{gfp}* and *Foxp3^{CNS2-gfp}* (CNS2) iTreg cells pretreated with or without ASC. Stability assay was performed as described in (Figure 2B) in the presence of DMSO (D) or JQ1 (2 μM; E). Data show means + SEMs of triplicates and represent 3 experiments.

(F) Quantification of Foxp3 transcripts in iT_{reg} cells described above by RT-qPCR. Data show triplicates represent 2 experiments.

(G) Quantification of nascent Foxp3 transcripts in iT_{reg} cells upon acute JQ1 treatment. Data show triplicates and represent 2 experiments.

Unpaired, two-tailed t test.

See also Figure S4.

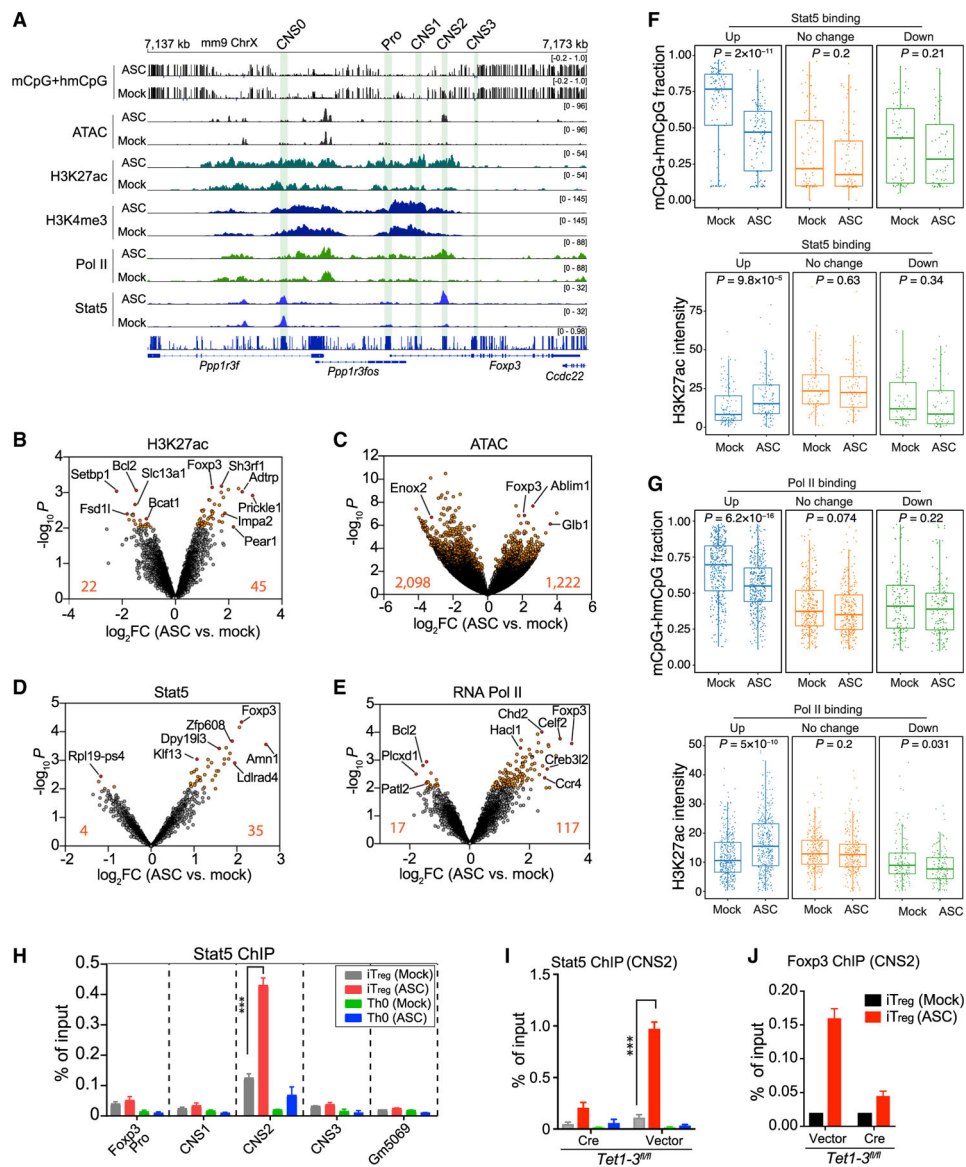


Figure 5. DNA methylation controls chromatin accessibility and nuclear factor binding at CNS2 (A) Epigenetic modifications and RNA Pol II and Stat5 binding around the *Foxp3* locus in mock- and ASC-treated *iT_{reg}* cells. Data represent 2 biological replicates.

(B-E) Effects of ASC on H3K27ac (B), chromatin accessibility (C), and Stat5 (D) and RNA Pol II binding (E) in *iT_{reg}* cells after 4 d treatment. Data were pooled from 2 biological replicates. Differentially represented peaks are highlighted and counted ($p < 0.01$).

(F and G) Cross comparison of the levels of mCpG and H3K27ac in regions showing differential ($p < 0.05$) Stat5 (F) or RNA Pol II (G) binding in ASC- versus mock-treated *iT_{reg}* cells. Unpaired two-samples Wilcoxon test.

(H) Stat5 ChIP-qPCR with mock- and ASC-treated *iT_{reg}* and Th0 cells after 30 min of IL-2 stimulation. Data represent 2 experiments.

(I and J) Stat5 (I) and Foxp3 (J) ChIP qPCR at CNS2 in *iT_{reg}* cells upon acute deletion of *Tet1-3* followed by ASC treatment. *Tet1-3^{fl/fl}* CD4 Tn cells were transduced with retroviral

Cre 1 d after activation. ASC or PBS was added to media at d 3. Transduced cells were sorted 3–4 d later for ChIP qPCR. Data show means + SEMs of triplicates and represent 2 experiments.

See also Figure S5.

Author Manuscript

Author Manuscript

Author Manuscript

Author Manuscript

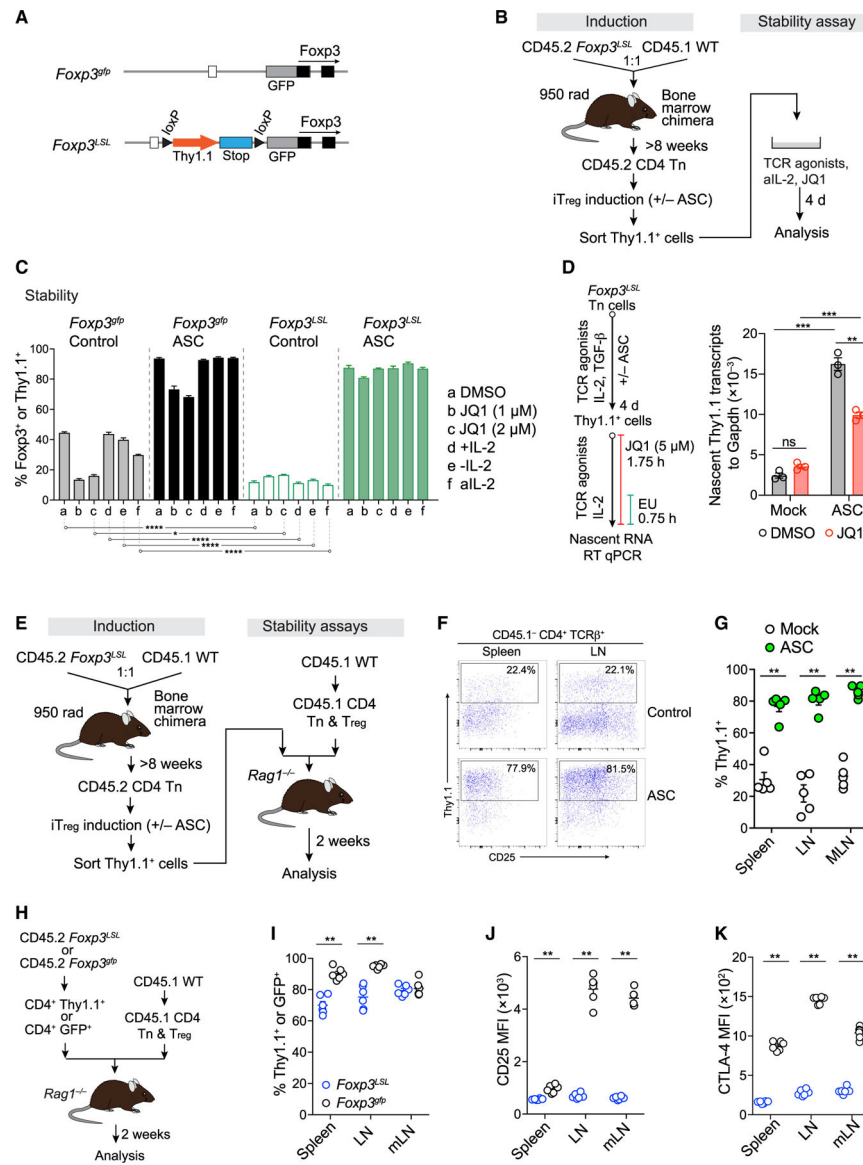


Figure 6. Assessment of the role of Foxp3 feedforward loop in maintaining Foxp3 transcription and Treg cell fitness

(A) Schematic of *Foxp3^{gfp}* and *Foxp3^{SL}* knockin mice.

(B) Experimental procedures for Thy1.1 induction and stability assays *in vitro*.

(C) Stability of Foxp3 expression in iTreg cells and Thy1.1 expression in wannabe iTreg cells pretreated with or without ASC. Data show means + SEMs of triplicates and represent 2 experiments.

(D) Quantification of nascent Thy1.1 transcripts in wannabe iTreg cells upon acute JQ1 treatment by EU pulse labeling and RT-qPCR. Data represent 2 experiments. Unpaired, two-tailed t test.

(E) Experimental procedures for assessing the stability of Thy1.1 expression in wannabe iTreg cells *in vivo*.

(F and G) Thy1.1 expression in recovered live CD45.1⁻CD4⁺TCR β ⁺ cells. n = 5 each group. LN, lymph node; MLN, mesenteric lymph node. Data represent 2 experiments. Mann-Whitney test.

(H–K) Assessment of the stability of Foxp3 or Thy1.1 transcription in nT_{reg} or wannabe T_{reg} cells *in vivo*. The percentages of GFP⁺ or Thy1.1⁺ cells among live CD45.1⁻CD4⁺TCR β ⁺ cells (H, I) and CD25 (J) and CTLA-4 (K) MFIs were calculated in live GFP⁺ or live Thy1.1⁺ cells. n = 6 each group. Data represent 2 experiments. Mann-Whitney test. See also Figure S6.

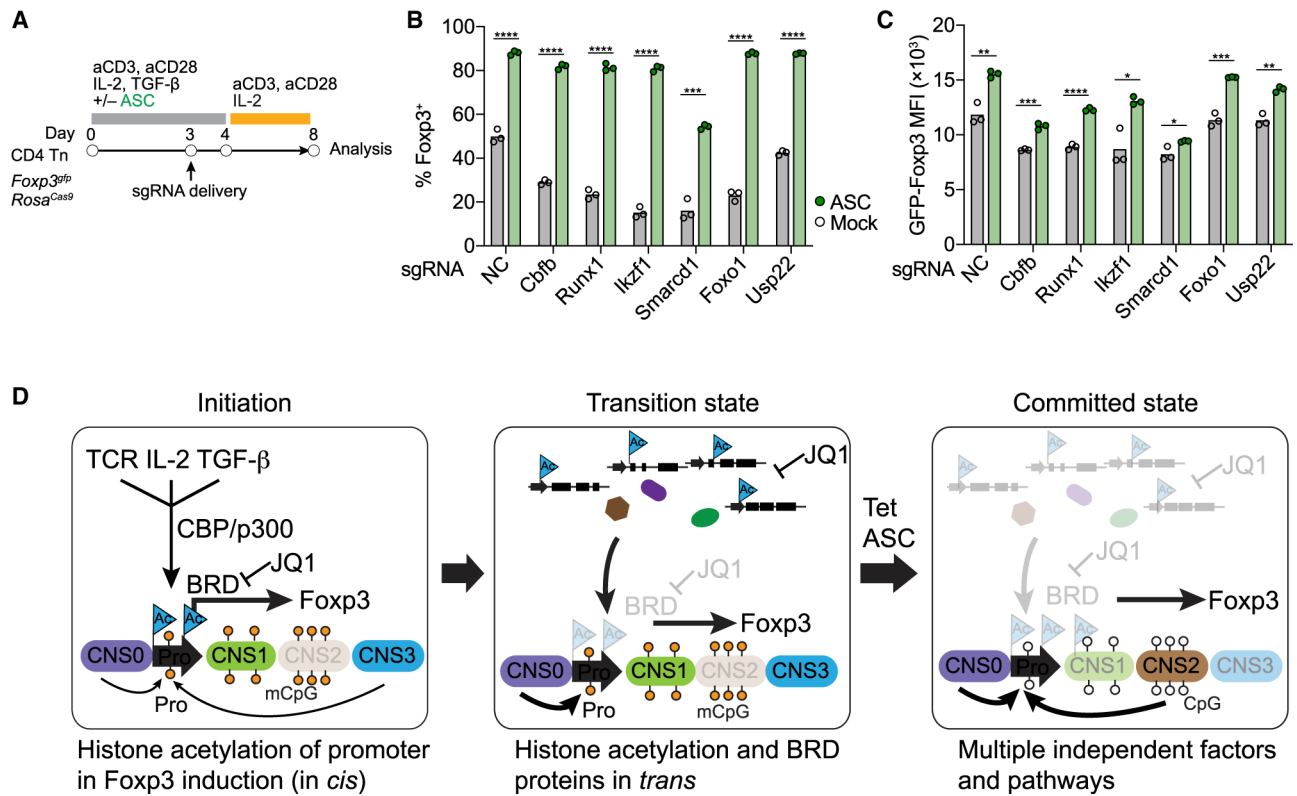


Figure 7. Multiple pathways regulate the stability of Foxp3 expression in fully differentiated iT_{reg} cells

(A–C) Foxp3 expression in iT_{reg} cells upon CRISPR knockdown of known regulators. CD4 Tn cells isolated from *Foxp3^{gfp} Rosa^{Cas9}* mice were cultured in T_{reg}-induction media with or without supplemented ASC. Cells were transduced by retroviral sgRNA at d 3 and GFP-Foxp3⁺ cells were sorted at d 4 to assay the stability of Foxp3 expression (A). Live cells were gated to quantify Foxp3⁺ cells (B) and Foxp3 MFI (C). NC, non-targeting control sgRNA. Data show triplicates and represent 2 experiments. Unpaired, two-tailed t test. (D) A model of transcriptional drivers of Foxp3 expression during iT_{reg} cell development. At the initiation stage, T_{reg}-induction cues deposit histone acetylation at *Foxp3* promoter to promote Foxp3 transcription. During the transition state before Tet-induced DNA demethylation, Foxp3 transcription is maintained by histone acetylation signal in *trans* via multiple positive regulators. After DNA demethylation, both *cis* and *trans* mechanisms of histone acetylation signal are dispensable for maintaining Foxp3 expression. Ac, histone acetylation.

KEY RESOURCES TABLE

Reagent or resource	Source	Identifier
Antibodies		
AF488 anti-CD90.1(Thy1.1) (Clone: OX-7)	BioLegend	Cat#202506
APC anti-CD44 (Clone: IM7)	Thermo Fisher Scientific	Cat#17-0441-82
Biotin anti-CD90.1(Thy1.1) (Clone: OX-7)	BioLegend	Cat#202510
BV711 anti-CD4 (Clone: RM4-5)	BioLegend	Cat#100550
BV785 anti-CD25 (Clone: PC61)	BioLegend	Cat#102017
CD45.1 (Clone: A20)	BioLegend	Cat#110724
eFluor780 Fixable Viability Dye	Thermo Fisher Scientific	Cat#65-0865-18
eFluor450 anti-CD4 (Clone: RM4-5)	Thermo Fisher Scientific	Cat#48-0042-82
FITC anti-CD25 (Clone: PC61)	BioLegend	Cat#102006
FITC anti-Foxp3 (Clone: FJK-16 s)	Thermo Fisher Scientific	Cat#11-5773-82
PE anti-CD152(Ctla-4) (Clone: UC10-4B9)	BioLegend	Cat#106306
PE anti-CD4 (Clone: RM4-5)	BioLegend	Cat#100512
PE anti-mouse IgG2a	Jackson ImmunoResearch	Cat#115-115-206
PE Streptavidin	Tonbo Biosciences	Cat#50-4317-U500
PE-Cy7 anti-CD25 (Clone: PC61)	BioLegend	Cat#102016
PE-Cy7 anti-CD62L (Clone: MEL-14)	BioLegend	Cat#104418
Purified anti-CD90.1(Thy1.1) (Clone: HIS-51)	BD Biosciences	Cat#554892
Purified anti-mouse CD3 (Clone: 145.2C11)	Bio X Cell	Cat#BE0001
Purified anti-mouse DC28 (Clone: 37.51)	Bio X Cell	Cat#BE0015
Purified anti-mouse IL-2 (Clone: JES6-54H)	Bio X Cell	Cat#BE0042
Purified anti-mouse IL-2 (Clone: S4B6-1)	Bio X Cell	Cat#BE0043
Rabbit IgG	CST	Cat##2729S
Rabbit mAb anti-histone H3K27ac	Abcam	Cat#ab4729
Rabbit mAb anti-Stat5 (Clone: D2O6Y)	CST	Cat#94205
Rabbit pAb anti-Foxp3	Abcam	Cat#ab150743
Rabbit pAb Anti-RNA polymerase II CTD repeat	Abcam	Cat#ab26721
Rabbit pAb Anti-RNA polymerase II CTD repeat YSPTSPS (phospho S5)	Abcam	Cat#ab5131
Rabbit pAb Anti-RNA polymerase II CTD repeat YSPTSPS (phospho S2)	Abcam	Cat#ab5095
Bacterial and virus strains		
Stable Competent <i>E. coli</i>	NEB	Cat#C3040I
Chemicals, peptides, and recombinant proteins		
(+)-JQ1	Sigma-Aldrich	Cat#SML1524
Ascorbic acid 2-phosphate	Sigma-Aldrich	Cat#A8960
BioMag Plus Concanavalin A	Bangs Laboratories, Inc.	Cat#BP531
C646	Sigma-Aldrich	Cat#SML0002
DSG Cross Linker	Thermo Fisher Scientific	Cat#20593
GlycoBlue Coprecipitant	Thermo Fisher Scientific	Cat#AM9515

Reagent or resource	Source	Identifier
I-BET151	Sigma-Aldrich	Cat#SML0666
I-CBP112	Sigma-Aldrich	Cat#SML1134
Recombinant human IL-2	Frederick National Laboratory for Cancer Research	
Recombinant human TGF- β	R&D Systems	Cat#240-B-002
Recombinant mouse IL-4	PeptoTech	Cat#214-14
Recombinant mouse IL-6	PeptoTech	Cat# 216-16
SGC-CBP30	Sigma-Aldrich	Cat#SML1133
Critical commercial assays		
Accel-NGS Methyl-Seq DNA Library Kit	Swift Biosciences	Cat#30024
AMPure XP for PCR purification	Beckman Coulter	Cat#A63880
CellTrace Violet Cell Proliferation Kit	Thermo Fisher Scientific	Cat#C34571
Nextara DNA Library Prep Kit	Illumina	Cat#15028212
Click-iT Nascent RNA Capture Kit	Thermo Fisher Scientific	Cat#C10365
Dynabeads Mouse T-Activator CD3/CD28	Thermo Fisher Scientific	Cat#11452D
Dynabeads Protein A beads	Thermo Fisher Scientific	Cat#10001D
Dynabeads Protein G beads	Thermo Fisher Scientific	Cat#10009D
EasySep Mouse CD4 T Cell Isolation Kits	STEMCELL	Cat#19767
Foxp3 / transcription factor staining buffer set	Thermo Fisher Scientific	Cat#00-5523-00
KAPA Hyper Prep Kit	Roche	Cat#KK8500
NEBNext Library Quant Kit	NEB	Cat#E7630S
PowerUp SYBR Green Master Mix	Thermo Fisher Scientific	Cat#A25779
SLAMseq Kinetics Kit – Anabolic Kinetics Module	Lexogen	Cat#061.24
SPRIselect	Beckman Coulter	Cat#B23318
SuperScript VILO cDNA Synthesis Kit	Thermo Fisher Scientific	Cat#11754050
TransIT-293 Transfection Reagent	Mirus	Cat#MIR 2705
TRIzol reagent	Thermo Fisher Scientific	Cat#15596026
NucleoSpin Gel and PCR Clean-up kit	MACHEREY-NAGEL	Cat#740609
truChIP Chromatin Shearing Kit	Covaris	Cat#520154
Phenol/Chloroform/Isoamyl Alcohol, 25:24:1	Calbiochem	Cat#516726
Deposited data		
All raw and analyzed data	This paper	GEO: GSE146250
ATAC-Seq	This paper	GEO: GSE146209
WGBS	This paper	GEO: GSE146248
ChIP-seq and Cut&Run-seq	This paper	GEO: GSE146442
SLAM-seq	This paper	GEO: GSE162805
Experimental models: Cell lines		
Platinum-E	Cell Biolabs, Inc.	Cat#RV-101
Experimental models: Organisms/strains		
B6 CD45.1	The Jackson Laboratory	Stock #002014
<i>Foxp3^{gfp}</i>	Alexander Rudensky	Reference (Fontenot et al., 2005)
<i>Foxp3^{LSL}</i>	Hu et al.	Reference (Hu et al., 2021)

Reagent or resource	Source	Identifier
<i>Foxp3^{Cre} CNS2-gfp</i>	Alexander Rudensky	Reference (Feng et al., 2014; Zheng et al., 2010)
<i>Foxp3^{Cre} CNS0-gfp</i>	Dikiy et al.	Reference (Dikiy et al., 2021)
<i>Rosa^{Cre} Cas9</i>	The Jackson Laboratory	Stock #026179
<i>Rosa^{Cre} Foxp3^{gfp}</i>	This paper	
<i>Tet1^{fl/fl} Tet2^{fl/fl} Tet3^{fl/fl} (Tet1-3^{fl/fl})</i>	Jacob Hanna	Reference (Herzig et al., 2017)
Oligonucleotides		
Primers for cloning U6-sgRNA cassette (see Table S1)	This paper	N/A
Primers for amplicon-based bisulfite sequencing (see Table S1)	This paper	N/A
Primers for ChIP qPCR (see Table S1)	This paper	N/A
Primers for RT-qPCR (see Table S1)	This paper	N/A
Primers for quantifying <i>Tet2</i> and <i>Tet3</i> deletion (see Table S1)	This paper	N/A
sgRNA sequences (see Table S1)	This paper	N/A
Recombinant DNA		
pCAG-Eco	Addgene	Cat# #35617
pCl-Eco	Addgene	Cat# 12371
pMigR1-Cre-IRES-Thy1.1	Feng et al.	References (Feng et al., 2015)
pSIR-DsRed (BbsI)	This paper	
pSIR-DsRed-Express2	Addgene	Cat#51135